LEHRSTUHL FÜR TECHNISCHE THERMODYNAMIK
FRIEDRICH-ALEXANDER-UNIVERSITÄT ERLANGEN-NÜRNBERG
Professor Dr.-Ing. Stefan Will

Bachelorarbeit

von

Cortés Martín, Irene

Raman Spectroscopic Analysis of CO$_2$-Water Mixtures Containing Kinetic Hydrate Inhibitors

Betreuer: M.Sc. Christine Holzammer
Prüfer: Prof. Dr.-Ing. Andreas Braeuer

Bachelorarbeit
BA16_3

Matrikelnummer: 22208065
Studienrichtung: Chemie-und Bioingenieurwesen

Friedrich-Alexander-Universität Erlangen-Nürnberg

2016

Ich erkläre hiermit, dass ich die vorliegende Arbeit selbstständig verfasst und keine anderen als die angegebenen Quellen und Hilfsmittel verwendet habe. Ich versichere, dass die Arbeit in gleicher oder ähnlicher Form noch keiner anderen Prüfungsbehörde vorgelegt wurde und daher noch nicht als Teil einer Prüfungsleistung angenommen wurde.

Erlangen, den 25. Juli 2016

Index

Abbreviations and Symbols

Abbreviations

Abbreviations sorted alphabetically.

Abbreviations	Name
AA	Anti-agglomerates
BEG	Mono Butyl Glycol Ether
DEG	Diethylene Glycol
GH	Gas Hydrate
HF	Hydrate Formation
HSE	Health, Safety and Environment
IPR	Isosbestic Point Relation
IR	Infrared
KHI	Kinetic Hydrate Inhibitor
LDHI	Low Dosage Hydrate Inhibitor
MEG	Monoethylene Glycol
MeOH	Methanol
PVCap	Polyvinylcaprolactam
PVP	Polyvinylpyrrolidone
sI	Structure I
sII	Structure II
sH	Structure H
SHB	Strongly hydrogen-bonded
TBAB	Tetrabutylammoniumbromide
TEG	Triethylene Glycol
THI	Thermodynamic hydrate inhibitors
VCap	Vinylcaprolactam
VIMA	N-methyl-N-vinylacetamide
VP	Vinylpirrolidone
WHB	Weakly hydrogen-bonded

Symbols

Symbols sorted alphabetically.

Latin Symbols	Name	Units (SI)
G	Gibbs energy	$J \cdot mole^{-1}$
h	Plank constant	$J \cdot s$
H	Enthalpy	J
$\Delta H_{melting}$	Pure solvent melting heat	$J \cdot mole^{-1}$
K_H	Hammerschmidt constant	-
M	Molecular weight	$g \cdot mole^{-1}$
R	Universal gas constant	$J \cdot mole^{-1} \cdot K^{-1}$
S	Entropy	$J \cdot K^{-1}$
T	Temperature	K
ΔT	Freeze point depression	K
T_m	Melting point temperature	K
V_O	Initial frequency	s^{-1}
$\pm v_r$	Raman frequency	s^{-1}
W	Inhibitor weight percent	-
X	Molar fraction	mole/mole

Greek Symbols	Name	Units (SI)
$\gamma_{equilibrium}$	Stability grades	-
λ	Wavelength	nm
ν_R	Raman shift	cm^{-1}
ρ	Density	$kg \cdot m^{-3}$

Acknowledgements

This thesis would not have been successful without my supervisor, Christine Holzammer who gave me an opportunity to do this research work. I wish to express gratitude to her for his abundantly helpful and offered invaluable assistance, support, guidance throughout the study and especially for her patience.

I would also like to convey thanks to my colleagues at Erlangen Graduate School in Advanced Optical Technologies (SAOT) and special thanks to Medhanie Tesfay Gebrekidanfor let me measuring with the IR laser.

It is a pleasure to thank my friends that I met in Erlangen this year and the ones that have been with me for a long time for their warm and moral support.

Last but not the least, I wishes to express my love and gratitude to my beloved family for their unconditional and endless love.

1. Introduction

Natural gas industry has always noticed snow-like solid matter develops in pipelines used for gas transport. The movement of gas through the pipelines tends to push these snow-like materials together until they fuse to form plugs that may eventually block the pipelines [1]. Then, researchers discovered that these snow-like materials were natural gas hydrates that not only block the pipelines as it can be shown in figure 1.1, they can also endanger oil and gas production installations and the personnel that work in them.

This is because hydrates may agglomerate into a plug that divides the pipe segment into two pressure sections, with the section upstream of the plug being under high pressure and the section downstream of the plug being under low pressure. A rupture can occur in the high-pressure section or the pressure differential may become large enough to propel the plug as a solid projectile thorough the pipe segment, which can be very dangerous, and can lead to major incidents including loss of lives [2].

Figure 1.1 Formation of gas hydrate plugged in a subsea pipeline. Picture from Petrobras (Brazil) [3]

Natural gas hydrates are formed by water and small hydrocarbon molecules having a molecular diameter of less than 9 Å, under appropriate conditions of temperature and pressure [4]. Each of these hydrocarbon guest molecules are encage within a specific shape and size of cavity formed by hydrogen bonded water molecules. The hydrocarbon molecules, which commonly form hydrates, include methane (CH_4), ethane (C_2H_6), propane (C_3H_8) and isobutane (C_4H_{10}) [5]. The conditions under which hydrates form include low temperatures (typically less than 300 K) and moderate-to-

high pressure (typically more than 0.6 MPa) [4]. Thus from a knowledge of the chemical composition requirements and the thermodynamics of natural gas hydrates formation, the industry tries to prevent hydrates by the following ways [5, 6]:

- Drying the natural gas (dehydration)
- Heating the gas to a temperature above the hydrate equilibrium temperature at the operating pressure
- Compressing the gas only to pressures below the equilibrium pressure at the operating temperature
- Using chemical inhibitors

Traditional chemical inhibitors such as methanol, ethylene glycol and triethylene glycol are referred to as thermodynamic inhibitors because they act by modifying the equilibrium curve such that hydrate can no longer form at the operating temperature and pressure [7]. One of the challenges with using these inhibitors is that they are required in high concentration (up to 50 wt. %) with large attendant cost [8]. Furthermore, the oil and gas industries continue to move into deeper waters and conditions are getting extreme. Because of that reasons, thermodynamic hydrate inhibitors show limits to these kinds of usages.

Nowadays, newer forms of hydrate inhibitors have spread in the commercial market such as kinetic inhibitors and anti-agglomerants are required at much lower concentrations (effective at concentrations below 1 wt. % [8]).

These forms of inhibitors, collectively referred to as low dosage inhibitors, which prevent hydrates from adhering together to form significantly large solids (anti-agglomerants) or do not prevent hydrate nucleation but delay their formation (kinetic inhibitors) [9, 10].

2. State of the art

For the successful development of this project, here are explained some of the latest researches done about the main topics: Kinetic hydrate inhibitors (KHIs) and Raman spectroscopy applications.

Firstly, some field tests have performed to determine the potential of a range of KHIs under different field conditions. PVP (Polyvinylpyrrolidone) was used in three gas

wells and 800 m long gas line at the South-Western Wyoming field. PVP was found to be a suitable replacement for methanol, only if fluids are not too far from the hydrate region and/or the residence time (average amount of time that a particle spends in a particular system) is less than a few minutes. If a higher sub cooling is required, other KHIs should be considered [11].

VIMA/VCap (N-methyl-N-vinylacetamide/vinylcaprolactam) copolymer has been using in the West Pembina field in Alberta, Canada. The copolymer successfully inhibits the formation of hydrates in the oil pipeline operated by Imperial Oil Resources. Exxon has used the VIMA/VCap copolymer for field trials in the Gulf of Mexico. The copolymer was found to be compatible with various field facilities, and due to the lower liquid production and the copolymer dosage rate, a foaming tendency was not observed [11].

The VIMA/VCap copolymer has been used in a 4-inch flow line located in the Gulf of Mexico. The gas produced was mainly methane and the salinity of the brine was 6.1 wt. %. The use of the copolymer reduced the chemical treatment cost to 40% of the methanol injection process. In addition, the logistics is much simplifying due to the low quantity of the inhibitor used. The copolymer has also been used at an oil field located on the northern coast of Peru. The use of the copolymer resulted in a cost reduction of 55% over the previously used methanol injection process. Due to the high flash point and low toxicity of VIMA/VCap, potential hazards were also easing. Unlike methanol, the copolymer is compatible with paraffin wax, which is used as a corrosive inhibitor, and other field chemicals. In another field application, the VIMA/VCap copolymer was used in a gas field in Texas resulting in a 16% saving of chemicals and 50% reduction of chemical volumes [11].

Secondly, one of the spectroscopic techniques with the highest development since de 80s is Raman spectroscopy [12]. This is because of its versatility and simplicity in the sample preparations. Some of the applications are at biomedical and pharmaceutical fields, because it can carry out non-destructive measurements in biological tissues. These ones are relating to in-vivo and in-vitro skin studies [13, 14], cancer identification [15], etc. It is also important in forensic fields such as explosive and drugs identification [16] due to the capacity of analyzing small samples (picomolar scale).

Furthermore, Raman spectroscopy has a high sensibility while measuring carbon bonds. That is why; this method is used at polymeric applications for the study of the chemical bonds, in particular to polymeric chains (monomers and polymers). In these cases, the information given about the crystallinity and density is helpful to the control of the polymeric reactions [17]. For the same reason as the last field, Raman spectroscopy is also very useful in nanotechnology and the study of new material such as carbon nanotubes and graphene [18].

However, what is more important in this project are the oil and gas industries, not only in the study of the influence of inhibitors but also in the different phases of the production and manufacturing of the oil and polymers [19]. Due to the ease in-line installation and the low cost of the analysis, Raman spectroscopy is an attractive option in monitoring and controlling petrol and gas industry processes.

Through this project will be demonstrated how sensible is Raman spectroscopy to hydrogen bonds and the utility that this has in the study of clathrates and inhibitors [20, 21].

Nevertheless, this is not the end, because Raman spectroscopy has more applications on wide variety of fields like art, archaeology, geology, environmental protection, etc. [12].

2.1. Objectives

The aims of this project were focus on the traineeship of the Raman equipment, acquiring the basic knowledge of Raman scattering and the ways for preventing gas hydrates.

The first objective was making an identification and evaluation of the component's structures of the inhibitors plotted in the Raman spectra. The identification of the main peaks of the spectra and the relation with the stretching gives relevant information about the future behavior of the inhibitors.

However, the most relevant section is when the inhibitors are added to a sample with water and carbon dioxide. In these cases, the determination of the inhibitor's influence of a variety of parameters and correlation between all of them reveals significant information about the gas hydrate formation.

Likewise, searching for the differences between the different behaviors of the inhibitors and comparing their effectiveness provide information about how the inhibitors work and inhibit the gas hydrate formation.

3. Theoretical Background

3.1. Gas Hydrates

3.1.1. Gas hydrate structure and composition

Natural gas hydrates (GH) are crystalline solids composed of water and gas. The gas molecules (guests) are trapped in water cavities (host) that are composed of hydrogen-bonded water molecules. Typical natural gas molecules include methane, ethane, propane and carbon dioxide [5]. In nature, they appear undersea in the continental shelves and the permafrost regions [22, 23].
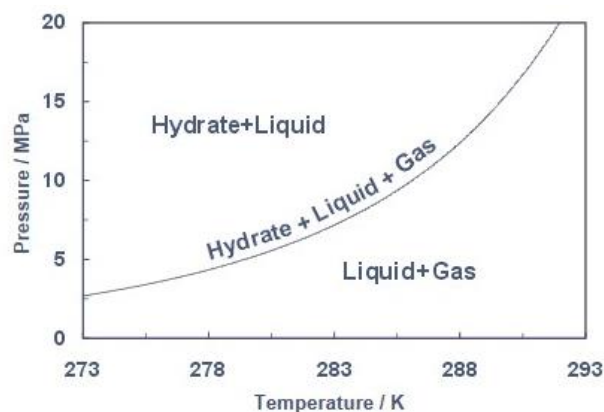
Figure 3.1 Pressure versus temperature phase diagram for methane hydrates [25]

GH are stable just at specific pressure and temperature conditions as it is shown in figure 3.1 where the temperature is typically less than 300K (almost ambient temperature) and the pressures are moderate (typically more than 0.6 MPa) [24]. In addition, it depends on other parameters such as the gas composition and the salinity of the water [24].

Gas hydrates are composed of approximately 85 mole% water, and therefore many of their properties are similar to those of ice such as physical appearance or density, whereas other properties contrast greatly with those of ice such as thermal conductivity and thermal diffusivity.

There are three main types of crystal structures for a gas hydrate, which are known as structure I (sI), structure II (sII), and structure H (sH).

Cubic structure I predominates in the Earth's natural environments, and contains small (0.4-0.55nm) guests while cubic structure II generally occurs with larger (0.6-0.7 nm) guests in mostly man-made environments. However, hexagonal structure (sH) may occur in either environment (natural and man-made), but only with mixtures of both small and large (0.8-0.9 nm) molecules. Most hydrate science, and thus most applications, concentrates on structure I and II, while structure H is anecdotal occurrence [4].

Hydrate crystal structure	I		II		H		
Cavity	Small	Large	Small	Large	Small	Medium	Large
Description	5^{12}	$5^{12}6^2$	5^{12}	$5^{12}6^4$	5^{12}	$4^35^66^3$	$5^{12}6^8$
Number of cavities per unit cell	2	6	16	8	3	2	1
Average cavity radius (Å)	3.95	4.33	3.91	4.73	3.91†	4.06†	5.71†
Coordination number*	20	24	20	28	20	20	36
Number of waters per unit cell	46		136		34		

*Number of oxygens at the periphery of each cavity.
†Estimates of structure H cavities from geometric models.

Figure 3.2 The three common hydrate unit crystal structures [5]

Figure 3.2 (a) shows the different cage types. The type of cage formation depends primarily on the size of the guest molecule. While methane fits into small and large cages of sI, propane is too large to fit into the large cage of sI but fit into the large cage of sII. Gas hydrates found in oil and gas pipelines are mainly sII because natural gas contains methane with small amounts of larger hydrocarbon molecules such as propane and isobutane [26]. Conversely, the majority of naturally occurring
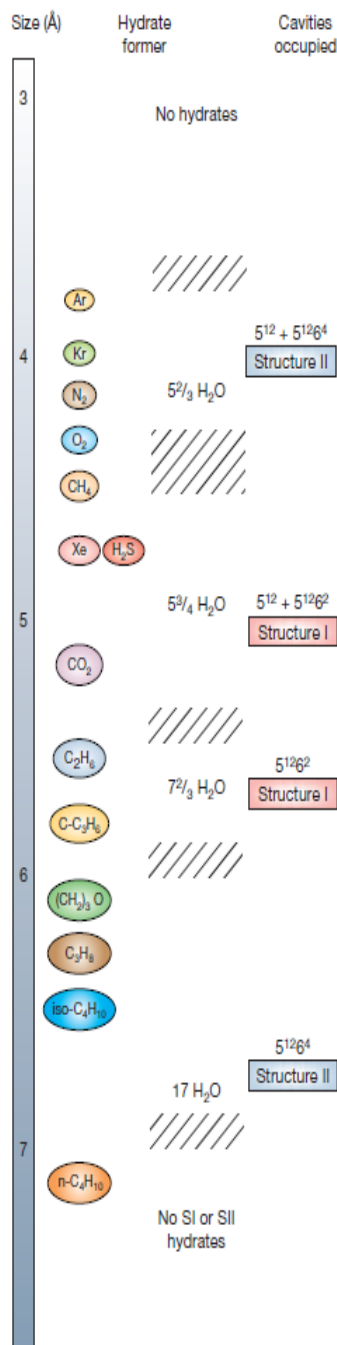
Figure 3.3 Hydrate guests versus hydrate cavity size ranges [5]

deposits of gas hydrates is sI because they are composed of methane (from biogenic sources) and do not contain heavier hydrocarbons. Exceptions are thermogenic hydrate deposits that contain heavier hydrocarbons and therefore they formed from sII and in rare cases sH [5].

Figure3.2 (b) shows the different hydrate structures and their associated cage types and some of the principal properties of each one. Structure I consists of two different cages, a small pentagonal dodecahedral cage, denoted 5^{12} (contains 12 pentagonal faces on the cage), and a large tetrakaidecahedral cage, denoted $5^{12}6^2$ (contains 12 pentagonal and 2 hexagonal faces on the cage). Structure II also includes the small 5^{12} cage in addition to a large hexacaidecahedral cage, denoted $5^{12}6^4$ (contains 12 pentagonal and 4 hexagonal faces on the cage). Structure H is composed of the small 5^{12} cage, a mid-sized $4^35^66^3$ cage (contains 3 square, 6 pentagonal, and 3 hexagonal faces on the cage), and a large icosahedral cage, denoted $5^{12}6^8$ (contains 12 pentagonal and 8 hexagonal faces on the cage) [5].

Gas hydrate are known as non-stoichiometric compounds because some of the cages in the structure can be vacant; however, a sufficient numbers of cages must be occupied by guest molecules for the gas hydrate to be stable [5]. In all three structures, typically there is only one guest molecule within each cage. Moreover, at unusual conditions such as very high pressure (>0.1 GPa) [5], it is possible to have multiple-cage occupancy with unusually small guests, such as hydrogen or noble gases. For example, hydrogen could form hydrates at very high pressure with as many as two occupants in the small cage and four in the large cage of hydrate sII [5]. However, very small guests and multiple occupancies are considered an aberration.

Remarkably, when all hydrate cavities are filled, the three crystal types have similar concentrations of components: 85 mole% water and 15 mole% guest(s). Hydrate formation is most likely to take place at the interface between the bulk guest and aqueous phases, because the hydrate component concentrations greatly exceed the mutual fluid solubilities. The solid hydrate film at the interface acts as a barrier to prevent further contact of the bulk-fluid phases, and fluid surface renewal is required for continued clathrate formation [4].

A number of researchers have commented on the fit of the guest molecule within the hydrate cage. The size ratio is not absolute for each cage; instead, it occurs over a molecular size range, which has a number of important implications. The implication is that clathrate hydrates have no fixed size ratio of guest to host, as shown by the ranges in figure 3.3. This figure represents the types of guests that fit in a cage while the size is increasing and the type of structure. At the smallest structure, the only guests that fit on the cage are noble gases, diatomic molecules and methane. In structure I, the molecules inside the guests can be little carbon chains such as ethane or butane. It is particularly interesting to note the resulting behavior of molecules at cage size borders [4].

3.1.2. Formation and dissociation

The freezing point of water is particularly high due to hydrogen bonds and the molecular arrangement in the solid phase takes regular and hexagonal shape. The presence of another compound in the proper conditions cause that the hydrogen bonds orientate over the second compound and consequently, a crystal (hydrate) forms. Hydrate nucleation and growth may have the same process as crystallization process such as precipitation of salt from solution.

An important parameter for a quicker formation is the agitation. GH formation is facilitated by higher fluid velocities thus to the turbulence which unsettle the mixture and start the separation. The susceptible regions with higher turbulence are pipelines, vessels or heat exchangers [6].

The earliest conceptual picture for hydrate nucleation is the labile cluster mechanism. A labile cluster is an unstable entity that readily undergoes change. The labile cluster are composed of a guest molecule surrounded by 20 and 24 (cf. 5^{12}, $5^{12}6^2$ cages of sI) or 20 and 28 (cf. 5^{12}, $5^{12}6^4$ cages of sII) water molecules in the first solvation shell.

This model considers either nucleation to occur by the agglomeration of labile clusters on the liquid or the vapor side of the interface. A modification of the labile cluster model is based on adsorption and clustering on the vapor side of the interface. An alternative and more recent mechanism is the local structuring hypothesis that focuses on the development of guest molecules being arranged (ordered) in configurations similar to that in the hydrate a hydrogen-bonded water network [5].

In the interest of keeping this section short, just the labile cluster nucleation hypothesis will be resumed. Gas hydrate formation is a time dependent process that can be divided into hydrate nucleation, hydrate agglomeration and growth, and finally dissociation [5]. Figure 3.4 shows the process of the gas hydrate formation. At favorable temperature and pressure conditions, water molecules form pentagonal structures. When the gas is dissolved into the water, the pentagonal structures hold together and surround the new guests. As a result, the water creates an envelope around the gas molecules, which are called labile cluster. This new tridimensional structures are metastable and that is why they grow and disperse until they reach the critical size and they agglomerate forming a gas hydrate.
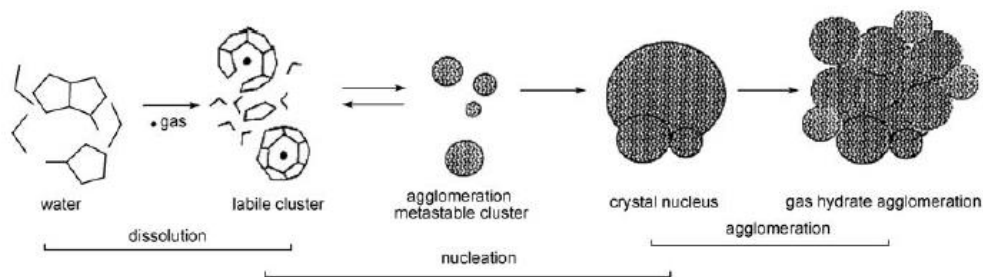
Figure 3.4 Hydrate formation hypothesis [5]

a. Hydrate nucleation

Hydrate nucleation is the process that produces a small labile cluster. It is called hydrate nucleus. This cluster consists of water and gas molecules. It grows, disperses and tries to grow again because a labile cluster is unstable and ready for continuous changing [5]. The general formation formula of a gas hydrate is expressed below by equation3.1.

$$M(g) + nH_2O(l) \leftrightarrow M \cdot nH_2O(s) \qquad (3.1)$$
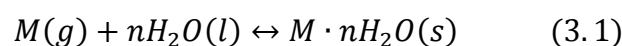
Where M is a natural gas molecules, n is the number of water molecules required to form a gas hydrate per one molecule of gas, and $M \cdot nH_2O$ is the gas hydrate [28, 29].

Imperfections in pipelines, pipe elbow, valves, etc. are prone places for the initiation of the nucleation. Generally, interface gas-water is a vulnerable place for the nucleation [24].

b. Hydrate agglomeration and growth

After the nucleation step, the crystal growth process occurs continuously and forms metastable clusters. The combination of three parameters should be considered. These are the kinetics of crystal growth at the surface of hydrate, mass transfer components to the growing surface, which is referred to the solubility equilibrium of the guest, and heat transfer away from the growing surface. This third parameter concerns to the fact that the hydrate nucleation is an exothermic reaction and consequently, the energy from the reaction should be removed in order to continue with the growth. Finally, when the crystal nucleus have the enough size, they agglomerates together and become a compact structure (clathrate).

c. Hydrate dissociation

Hydrate dissociation is an endothermic and vital process to eliminate hydrate crystal, which blocks pipelines in oil and gas industry. Thus, decomposition of gas hydrate to water and gas molecules can be successful by supplying external heat to destroy hydrogen bonds between water molecules and van der Waals interaction and between host and guest molecule [5]. There are different approaches that apply to mitigate a gas hydrate plug such as dehydration, heat management, and chemical inhibition [5, 30]. This is explained in more detail in the following section.

To sum up, figure 3.5 shows the hydrate labile cluster formation mechanism imposed on a pressure-temperature trace. From point 1, gas dissolves in water, consequently, the pressure is reducing linearly with temperature. There is no hydrate formation during 1 and 2 period, which is defined as induction time (nucleation time, induction period or lag time), because of metastability [5, 31].Induction time is time taken from entering to hydrate forming region and the onset of hydrate formation [32].Point 2 is the beginning of hydrate formation. Along point 2 and 3, pressure dramatically falls while a rapid hydrate growth takes place. This occurs until the end of growth for hydrate formation at point 3. Finally, when the temperature increases, hydrate dissociation starts simultaneously from point 3 to A. Hence, the pressure slightly increases at the beginning and then sharply rises until point A. This point is called the hydrate equilibrium temperature and pressure [5]. However, the information for the crystal growth rate after nucleation still being limited.

3.1.3. Methods to prevent gas hydrates formation

The industries can choose between four methods of hydrate prevention and control. These four methods are:

1. Gas dehydration
2. Maintaining an operating temperature higher than the hydrate equilibrium temperature
3. Operating at a pressure lower than the hydrate equilibrium pressure
4. Injecting a chemical inhibitor into the gas stream

These hydrate prevention and control strategies may be implemented in isolation or in combination depending on the specific circumstances of the field, especially as it relates to practicability and economics [7]. Generally, the use of chemical inhibitors is about the most common [33].
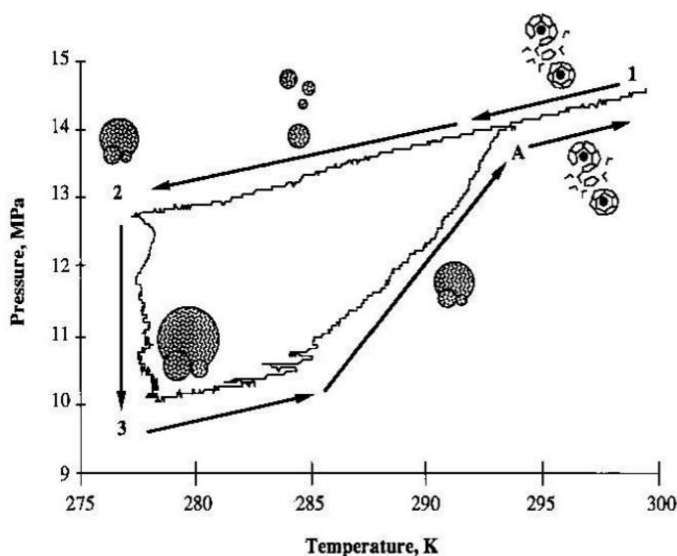
Figure 3.5 Diagram of temperature versus pressure trace for methane hydrate formation [31]

This involves injecting chemicals into the gas stream. For a detailed explanation, the different kinds of chemical inhibitors and properties, more information is given in the following section.

3.2. Inhibitors

This section highlights the major classes of gas hydrate inhibitors. The aim of including this section is to introduce the readers to common types of inhibitors, their relative advantages and disadvantages, and to provide an understanding about the evaluation of the performance of inhibitors [11].

Mainly, it is possible to divide the types of inhibitors into three different classes attended by physicochemical action: thermodynamic hydrate inhibitors, anti-agglomerates and kinetic hydrate inhibitors.

3.2.1. Thermodynamic hydrate inhibitors (TIHs)

The action of this kind of inhibitors corresponds with the direct relation of the thermodynamics on the system gas-water-hydrate. For some pressure, temperature and gas composition conditions, the free energy of the system reaches the minimum. The following thermodynamic equation3.2 describes the operation:

$$\Delta G = \Delta H - T\Delta S \qquad (3.2)$$

Where ΔH is the enthalpic term and ΔS is the entropy that are related to the molecules structuration and the relative order [24].

The thermodynamic inhibitors disturb the hydrogen bonds of water molecules and consequently, the entropic term of equation 3.2 increases to a higher negative value and at the end, the Gibbs energy becomes higher. This means that the original temperature and pressure conditions are less favorable at forming gas hydrates than before. In other words, thermodynamic inhibitors shift the hydrate formation equilibrium curve to lower temperature and higher pressure [20]. Polar components such as alcohols or glycols form hydrogen bonds with water and interfere with the internal order of water molecule and therefore, the formation temperature for hydrate gas decreases [24].

Around this type of inhibitors, the most widely used is methanol (MeOH) because of its efficiency and low prices but glycols such as monoethylene glycol (MEG) and

diethylene glycol (DEG) are also employed. Finally, some inorganic salts such as NaCl or MgCl$_2$ are effective inhibitors however; the corrosive problems that could damage the pipes restrict their usage [24].

A typical method to compare inhibitor's effectiveness is subcooling, defined as the difference between GH formation temperature with and without inhibitor. This measurement can be theoretically calculated though the freeze point depression in aqueous solution in the presence of a non-volatile solute. The mathematical expression (equation3.3) for the freeze point depression (ΔT)can be written as follows:

$$x_i = \frac{\Delta H_{melting}\Delta T}{RT_m^2} \qquad (3.3)$$

In which R is the universal gas constant, T_m is the melting point temperature, x_i is the solute (inhibitor) molar fraction and $\Delta H_{melting}$ is the pure solvent melting heat. Hammerschmidt developed another equation (equation 3.4), which predict the effects of an additive addition in the hydrate formation temperature as a function of concentration [24].

$$\Delta T = \frac{K_H W}{M(100 - W)} \qquad (3.4)$$

In which W is the inhibitor weight percent in the aqueous phase, M is the inhibitor molecular weight and K_H is an empiric constant that depends on the inhibitor [34]. An inconvenience of this expression is that it can only be used for concentrations below 30% in methanol weight and 20% in glycol weight [24].

K$_H$ values and molecular weights of inhibitors are given in table 3.1 [35].

Component	Molecular weight (M)	K$_H$
Methanol	32	2335
Ethylene Glycol	62,07	2700
Diethylene Glycol	106,12	4000
Triethylene Glycol	150,17	5400

Table 3.1 Physical constants of inhibitors

Figure 3.6 shows the how the weight percent of THIs can shift the equilibrium curves (γ$_{equilibrium}$) to different temperatures in methane hydrates. The tendency reveals that if inhibitor concentration increases, the stability grade also increases.
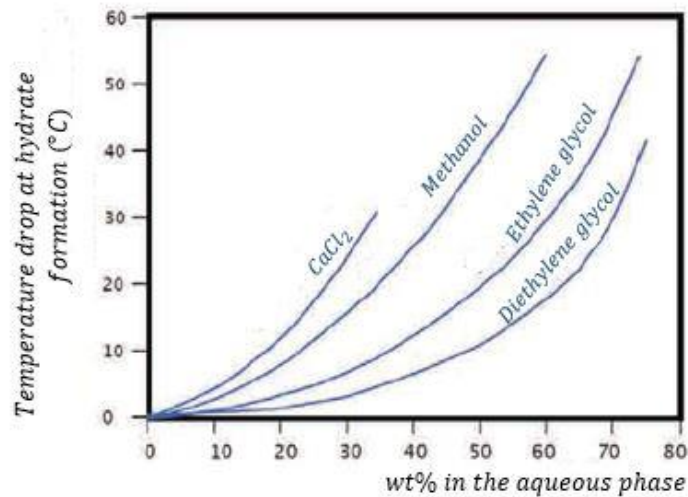
Figure 3.6 Shift of the equilibrium curve of the methane-water hydrate stability using thermodynamic inhibitors [24]

It is also important to say that to reach high stability grades is required an elevated inhibitor concentration (>10 wt. %).
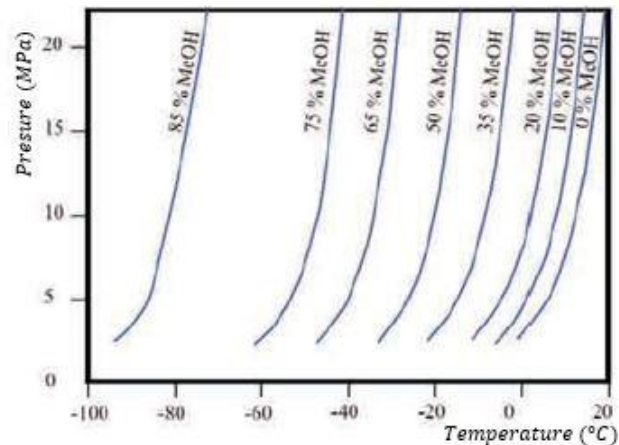
Figure 3.7 GH formation region shifts by the effect of methanol [24]

In general, thermodynamic inhibitors modify the hydrate formation region by displacing it towards higher-pressure values and lower temperature values in respect of the non-inhibitor system.Figure3.7 shows a pressure-temperature diagram where the concentration of the inhibitor (MeOH) is variable and how this change the GH formation region [24].

3.2.2. Low Dosage Hydrate Inhibitors (LDHIs)

A high number of researchers attempt to develop a new generation of chemicals because of the multiples THIs disadvantages: corrosion, Health, Safety and Environment (HSE) and high costs. The Low Dosage Hydrate Inhibitors (LDHIs) are the new developed inhibitors. LDHIs are divided into two main classes: Anti-agglomerates (AAs) and Kinetic Hydrate Inhibitors (KHIs). The main differences

between THIs and KHIs are the lower concentration needed for KHIs and the mechanism of hydrate inhibition [36].At present, combinations of KHIs and AAs are alternatives for delaying hydrate formation and hydrate plug prevention respectively [36].

a. Anti-Agglomerates (AAs)

Anti-Agglomerates are one of the LDHI classes. The effective concentration is lower than 1wt. % [37].Anti-agglomerates prevent the agglomeration of hydrate crystals into a large size. The development of gas hydrate formation still occurs, but the crystals do not plug and can be transported through the pipeline, because the size of the gas hydrate crystals is nanometric. However, they only work when a liquid hydrocarbon phase is present, i.e. crude oil or condensate.

AAs are less independent of time and the degree of subcooling of the system compared to kinetic hydrate inhibitors (which are explained in more detail hereafter) and that is why they are used in deep-water applications [8].

b. Kinetic Hydrate Inhibitors (KHIs)

Typically, kinetic hydrate inhibitors are water soluble polymers and they usually consist of other small organic molecules which are added for efficiency enhancement (synergists). KHIs generally have small cyclic amide groups as the active units as it is shown in figure 3.8[8, 37 and 38] and they do not affect the thermodynamic conditions of hydrate formation [11]. In fact, the purpose of KHIs is to delay gas hydrate nucleation and crystal growth [39].
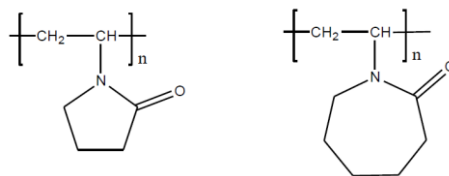
Figure3.8 Kinetic Hydrate Inhibitor. Polyvynilpirrolidone (PVP) (a) Poly(N-Vinylcaprolactam) (PVCap) (b) [39]

Several mechanisms have been proposed for the inhibition of gas hydrate formation by KHIs. One of the proposed mechanisms suggests that the perturbation of the water structure prevents the growth of hydrate particles to the critical size [7, 40]. Some studies suggested that the nucleation and/or crystal growth inhibition is achieved via adsorption on hydrate surface [41]. A third proposed mechanism

suggests that the polymer chains interfere with the nucleation and/or crystal growth of hydrates through an inhibitor-adsorption of guest molecules into the crystal lattice [42, 43].

Figure 3.9 shows one of those mechanisms. In this case, the polymeric chain is display in a crystal surface and the active groups are represented as black stars. When the critical nucleus size is achieved, the actives groups hold the nucleus (white stars) and consequently, the growth cannot begin.
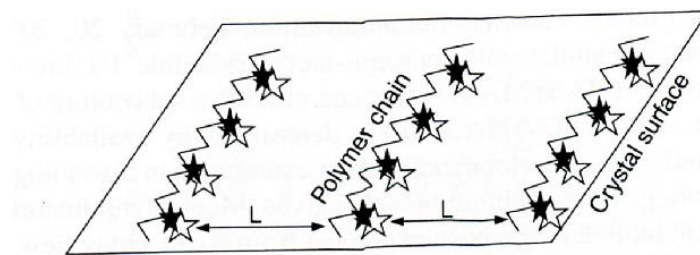
Figure 3.9 One mechanism for kinetic inhibitors [5]

The time taken for hydrate formation in the presence of KHIs is larger than the residence time of gas in transport facilities [44]. This time depends on the degree of subcooling. As it is explained at section 3.2.1; subcooling(ΔT), is the temperature difference between the hydrate dissociation temperature and the operating temperature at a given pressure, and is the driving force for the hydrate formation [37, 45].

The commercial KHIs generally have maximum subcooling around 9-10°C. The main advantage of KHIs is the low concentration usage (1 wt. %) [45]. Furthermore, KHIs are cleaner and safer than THIs for the environment and consequently, they are widely proliferating. The main drawback of this kind of inhibitors is that they can only be applied in moderate subcoolings (less than 13°C) [46].

3.3. Foundations of Raman spectroscopy

3.3.1. Introduction

Raman spectroscopy is a photonic high-resolution technique, which gives in a few seconds the chemical and structural information of almost every kind of material or organic/inorganic component. For this reason, it is capable of identifying them. Raman spectroscopy analysis works with a scattered light test at one material when a monochromatic beam of light strikes the sample.

A little light portion is inelastically scattered and it has small frequency modifications that are unique from the analyzed material and independent from the incident light frequency. This analysis technique is used directly on the sample; this means that it is not necessary to prepare the sample and that it is a non-destructive and non-invasive technique [47].

3.3.2. Raman Effect

A. Smekal theoretically predicted the Raman Effect in 1923, although, it was experimentally demonstrated for the first time by Sir Chandrasekhar Venkata Raman in 1928 [48].

Ions and atoms are chemically attached to form molecules and crystal lattice structures, which are subjected to constant vibrational and rotational movements. These oscillations take place because of certain frequencies that depend on the particle weight and the dynamic behavior of the chemical bonds. Each vibrational and rotational movement corresponds to a concrete molecular energy value.

The relation of the electronic, vibrational and rotational energy curves is shown in figure 3.10. This diagram shows that the energy difference between rotational states are much smaller than that of vibrational states, and the energy difference between vibrational states is much smaller than that of electronic states. That means that many vibrational states "belong" to the same electronic state, and that many rotational states belong to the same vibrational states.

Essentially, Raman spectroscopy analysis works with a monochromatic beam of light at a specific frequency ν_0, which strikes a sample with indefinite properties. Most of the scattered light shows the same frequency as the incident light, but a minor fraction with a ratio 10^7 times lower than the incident light, suffers a modification because of light-sample interaction. The light, which keeps constant frequency ν_0 is called Rayleigh scattering. Additionally, the scattered light, which has two different frequencies, is called Raman scattering. The new frequencies $+\nu_r$ and $-\nu_r$ are Raman frequencies, which depends on the chemical nature, phase of the sample
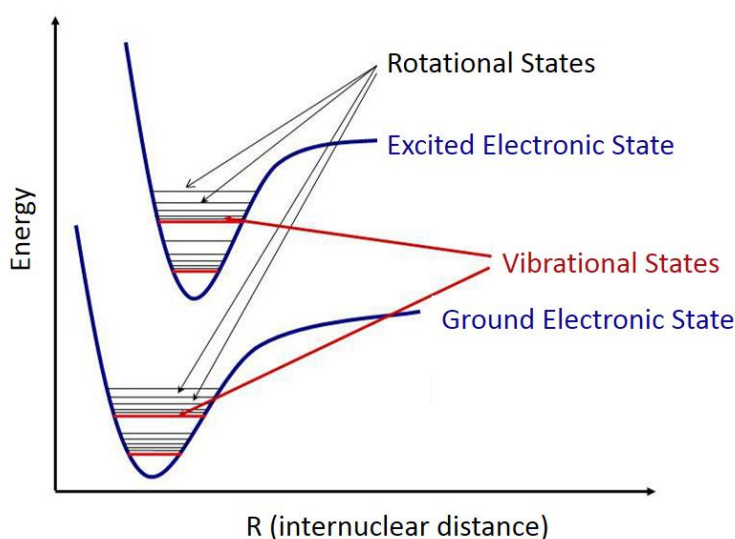
Figure 3.10 Energy states of a molecule

and the incident radiation [39]. Additionally, the difference between the incident and scattered frequencies ($\nu_0 + \nu_r$ and $\nu_0 - \nu_r$) just depends on the first and second parameter [46]. In figure 3.11, the electronic energy diagram is described in which a horizontal line represents an energy state.
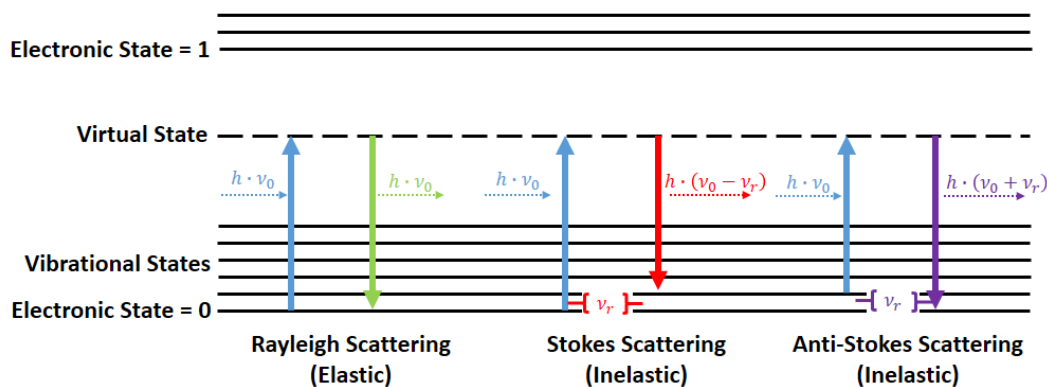
Figure 3.11 Energy level diagram related Raman scattering

When the incident photon energy $h \cdot v_0$ (where h is Plank constant) is bigger than the energy difference between two vibrational/rotational states, most of the photons go through the sample but a minor fraction is scattered. The scattering is caused by the incident photon, which induces the molecule to a transitory virtual energy state. The molecule leaves quickly the virtual energy state and stays in one of the allowed states, and simultaneously, it scattered a photon. The scattered photon frequency depends on the molecular transition [40].

On the one hand, if the result of the photon-molecule interaction is an incident photon with the same frequency, then it is an elastic collision owing to the fact that the molecule does not suffer any change. The incident photon has the same frequency v_0 and the molecule returns to the same energy level before the collision [40].This is called Rayleigh scattering.

On the other hand, if the result of the photon-molecule interaction is a scattered photon with a different frequency, then it is an inelastic collision because of the energy transference between the molecule and photon. In this case, it there are two possibilities [40]:

- When the frequency from the scattered photon is less than the incident is because the energy transfer goes from the photon to the molecule. This means that at the end, the molecule is at a higher state than before the collision. The scattered photon has a frequency $v_0 - v_r$ and this case is called Raman Stokes scattering.
- When the frequency from the scattered photon is higher than the incident is because the energy transfer goes from the molecule to the photon. This means that the molecule was at a higher state and after the collision, it returns to the fundamental state. The scattered photon has a frequency $v_0 + v_r$ and this case is called Raman Anti-Stokes scattering.

Raman shift $(v_r)$is typically expressed in wavenumbers, which have units of inverse length, as this value is directly related to energy. Equation 3.5 shows the calculation of the Raman shift:

$$v_r = \left(\frac{1}{\lambda_0} - \frac{1}{\lambda_1} \right) \qquad (3.5)$$

Where ν_r is the Raman shift expressed in wavenumber, λ_0 is the excitation wavelength, and λ_1 is the wavelength of the scattered photon. Most commonly, the unit chosen for expressing wavenumber in Raman spectra is inverse centimeters (cm^{-1}). Since wavelength is often expressed in units of nanometers (nm), the formula above can scale for this unit conversion explicitly.

As it can be seen in figure 3.12, a spectrum is represent by a main band (Rayleigh) and two secondary series, which correspond to Raman Stokes and anti-Stokes on both sides of Rayleigh band [39].
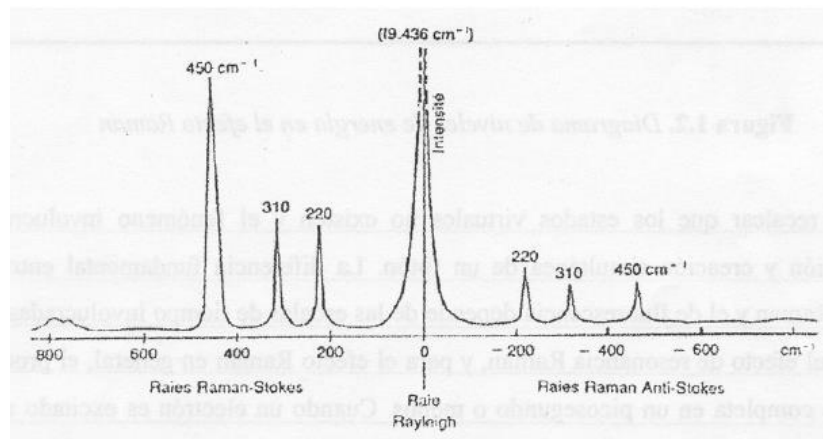
Figure 3.12 Rayleigh, anti-Stokes and Stokes bands [49]

At normal temperature and according to Maxwell-Boltzmann distribution energy law, 99% of the molecules are in the less energetic vibrational state, this means that the probability of Raman-Stokes scattering is higher than Raman anti-Stokes scattering. Raman Stokes scattering is around 100 times higher than Raman anti-Stokes scattering [47].

Along the next section, the writer is going to focus just on one spectrum, in concrete, the water spectra, which is clearly important to comprehend the basis of this work.

3.3.3. Raman spectrum: Liquid water

Because the main body of the samples is water, it has a relevant importance to study the water Raman spectra.

As it can be show in figure 3.13, when water is analyzed at different temperatures, the Raman spectra show a static point at approximately 3357 cm^{-1} that it is called isosbestic point. The scattered intensity under constant excitation power, and at a fixed Raman frequency, $\Delta\bar{v}$ cm^{-1} is constant and independent of the intensive

quantity, temperature, concentration, e.g., that gives rise to the spectral changes, for the pure liquid or solution studied [51].
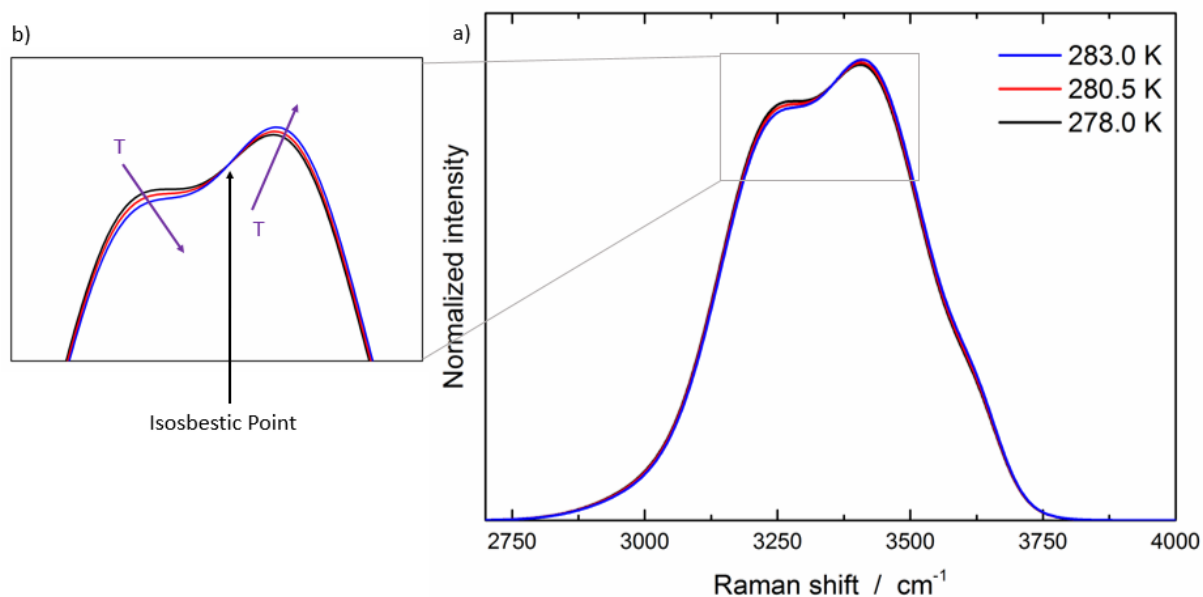
Figure 3.13 Raman spectra of liquid water at different temperatures (a), (b) shows a magnification between the Raman Shift 3150 and 3500 (Isosbestic Point)

According to the isosbestic point, it is possible to divide the spectra in two different sections in accordance with the strength of the hydrogen bonds.

As figure 3.14 shows at the left side until the isosbestic point is the Strongly Hydrogen-Bonded (SHB), which decreases their intensity when the temperature increases (figure 3.13) and after the isosbestic point to the right side is Weakly Hydrogen-Bonded (WHB), which increases their intensity when the temperature increases.
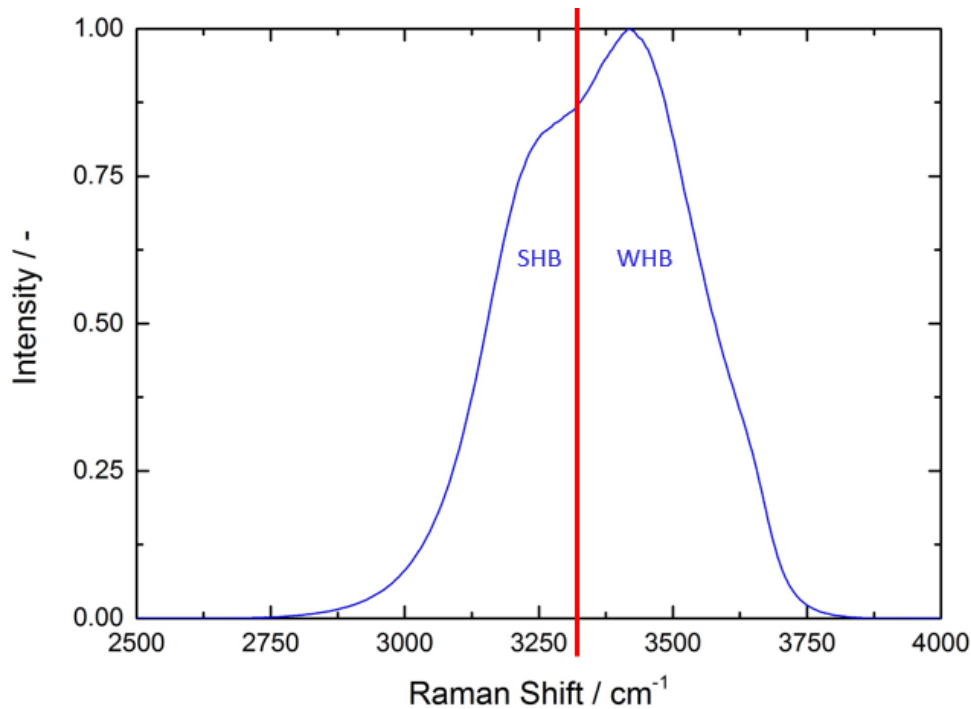
Figure 3.14 Raman spectra (liquid water) divided into the Strongly Hydrate-Bonded and the Weakly Hydrogen-Bonded.

Water spectrum should be modified with the use of THI inhibitors, but not when KHIs are used. In these cases, while SHB area decrease and WHB area increase; and consequently the area below the curve changes. This difference demonstrates that is less likely to form gas hydrate due to the hydrogen bond strength diminution.

It is easy to get the numerical data from the graph to obtain the result of the experiments. To be certainly sure, during these experimental exercises, two ways to calculate the relation between both sides of the spectrum were used.

1. Direct integration of the two areas below the curve.

$$Isosbestic\ Point\ Relation\ (IPR) = \frac{SHB\ area}{WHB\ area} \qquad (3.6)$$

2. The five peaks method: To evaluate the spectrum it is helpful to describe the spectrum as the sum of five Gaussian peaks. As it is shown in the following figure, the first and second peaks correspond to SHB section; and the last three peaks describe WHB section.
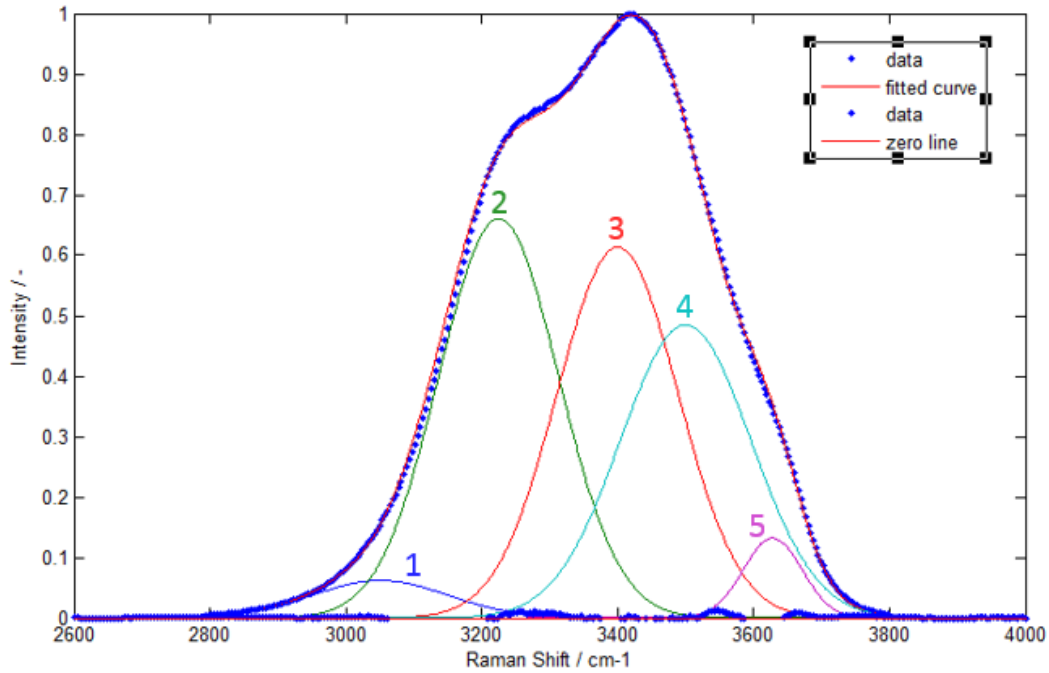
Figure 3.15 Decomposition spectrum into five Gauss peaks

By the creation of a new variable, a new relation between both sections can be built.

$$R = \frac{SHB}{WHB} = \frac{Peak\ 1 + Peak\ 2}{Peak\ 3 + Peak\ 4 + Peak\ 5} \quad (3.7)$$

In table 3.2 resumes the characteristics of the peaks: central wavelength and standard deviation.

N° of peak	Central wavelength	Standard deviation
1	3051	100
2	3225	88
3	3400	89
4	3500	96
5	3628	43

Table 3.2 Characteristics of the peaks: Central wavelength and standard deviation

4. Experimental

On this section, the writer will focus the attention on inhibitors and equipment description. Moreover, along the last sub-sections, the theoretical explanation and the procedure for the experiments are also described.

4.1. Chemicals

The chemicals used along the duration of this bachelor project were:

- Deionized water
- CO_2 (guest molecule)

Moreover, the inhibitors were:

a) HI-M-PACT HIW 85671 (Ethandiol and 2-butoxyethanol)
b) HI-M-PACT HIW 85610 (2-butoxyethanol)
c) HI-M-PACT 85232 HCW (2-butoxyethanol, ethandiol and quaternary ammonium compounds)
d) Luvicap BIO (PVCap copolymer in BGE)
e) Luvicap 55W (VP:VCap copolymer)
f) Luvicap PL (2H-Azepin-2-one, 1-ethenylhexahydro-homopolymer in ethanol)
g) Luvicap EG (low molecular weight PVCap in MEG)
h) Luvicap EG-HM (low molecular weight PVCap in MEG and quaternary ammonium compounds).
i) PVP (Polyvinylpyrrolidone)
j) TBAB (Tetrabutylammoniumbromide)
k) Starch, from potato

Where PVCap means polyvinylcaprolactam, MEG means monoethylene glycol, VP means vinylpirrolidone, and BGE means mono butyl glycol ether.

The relevant components and concentration of the chemicals are shown in table 4.1.

Chemical	Concentration (Component)
TBAB	50 wt. % solution in water
Luvicap EG	40 wt. % in MEG
Luvicap EG-HM	40 wt. % in MEG
Luvicap BIO	40 wt. % in BGE
HI-M-PACT HIW 85610	50-75 wt. % in water
HI-M-PACT HIW 85671	35-50 wt. % in water (ethandiol)
	10-20 wt. % in water(2-butoxyethanol)
HI-M-PACT 85232 HCW	35-50 wt. % in water (ethandiol)
	10-20 wt. % in water(2-butoxyethanol)

Table 4.1.Concentrations of the gas hydrate inhibitors

More detail information about security and some properties of each product are attached in *Appendix B. Safety Sheets*.

For this experiments is assume that all the guest molecule works in the same way, that is why CO_2 was chosen as a guest molecule and also because it specific properties such as low size, stable at high pressure and because it is safer than methane and propane which are flammable gases.
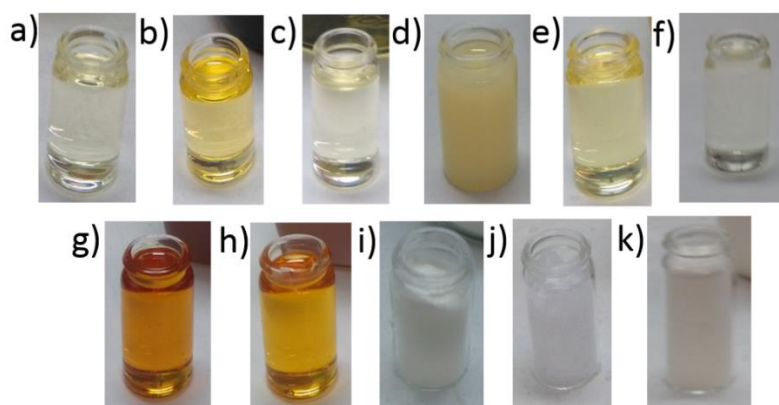
Figure 4.1 Inhibitor samples: HI-M-PACT HIW 85671 (a), HI-M-PACT HIW 85610 (b),HI-M-PACT 85232 HCW (c), Luvicap Bio (d),Luvicap 55 W (e),Luvicap PL (f),Luvicap EG (g), Luvicap EG HM (h),PVP (i),TBAB (j),Starch (k)

Figure 4.1 shows the inhibitors appearances. From (a) to (h) the inhibitors are liquids while the last three (PVP, TBAB and starch) are solids at normal conditions. From (a) to (e) the inhibitor's viscosity is comparable to the water while for Luvicap PL, EG and EG HM (f, g and h), the viscosity was higher and similar to honey. Another remarkable property of Luvicap Bio inhibitor (d) is that is almost opaque, and HI-M-PACT HIW 85610, Luvicap Bio, Luvicap 55 W, Luvicap EG and Luvicap EG HM (b, d, e, g and h) are yellow and brown colored. Finally, PVP and starch are powder while TBAB have a crystal structure.

For the optimal preparation of the mixtures, the writer gathers the information about the best proportion on the following references [11, 52-55]. The samples have the following composition as shown in table 4.2.

Sample	Inhibitor´s name	Inhibitor weight percent (wt.$_{inhibitor}$%)
a)	*HI-M-PACT HIW 85671*	1.064 wt. %
b)	*HI-M-PACT HIW 85610*	0.9695 wt %
c)	*HI-M-PACT 85232 HCW*	1.026 wt %
d)	*Luvicap Bio*	0.654 wt %

e)	*Luvicap 55 W*	0.648 wt %
f)	*Luvicap PL*	0.6017 wt %
g)	*Luvicap EG*	0.558wt %
h)	*Luvicap EG HM*	0.55 wt %
i)	PVP	0.0717 wt. %
j)	TBAB	0.4681 wt. %
k)	Starch	0.0684 wt. %

Table 4.2 Inhibitor weight percent of the samples using in this project

4.2. Experimental setup

In these experiments, inhibitor performance tests are carried out in a Raman scattering instrumentation. Figure 4.2 shows the entire equipment. The central part is the cell (C), which is connected to two pumps (Teledyne Isco syringe pumps model 260-D); one provides CO_2 (A) and the other provides water (B). There is also one more connection in case of inject manually the sample into the cell. The high-pressure variable volume view cell has four optical accesses and a piston to modify the volume (D).

In order to control the temperature, the cell has a double walled jacket in which a refrigerant can circulate though. A cryo compact thermostat CF41 by Julabo (F12-ED from Julabo) accomplishes the temperature regulation of the cell (E) and the temperature inside the cell was continuously measured with a Pt100 thermometer and recorded (F). In order to control the pressure,

Figure 4.2 Laboratory instrumentation

the cell has two sensors inside and for security reasons, one connection for pressure release in case of the pressure exceed the safety limit.

The cell has a connection to remove the gas, which guide the gas to the residual ventilation system. A screwed button located at bottom empties the cell from the liquids.

The cell has four windows, which are located 90° from one another. One of them is used for the optical setup. Because of the difference of temperature during the experiment, on this window was added a compressed air device to prevent water condense on the glass. The opposite one is blocked so the light cannot pass to the other side. A camera located on the third window monitors the inside and finally, the fourth window is free of devices.

Furthermore, inside of the cell, a magnetic agitator positioned at the bottom of the cell continuously agitates the liquid water-rich phase and thus assures a good mass transport between the liquid water-rich phase at the bottom of the cell and the liquid CO_2 rich phase at the top.

Finally, and in order to determine the influence of the external factors, the temperature of the room was measured by two sensors controlled by OMEGA TC-08. The first sensor (G) was at the same height of the table and the other one a little bit higher (H).

For the measurement, Raman sensor provides the Raman spectra from the liquid water rich phase in a backscattering arrangement. Individual Raman spectra are recorded in direct sequence. [52]. Figure 4.3 is a brief scheme of how the Raman scattering instrumentation works.
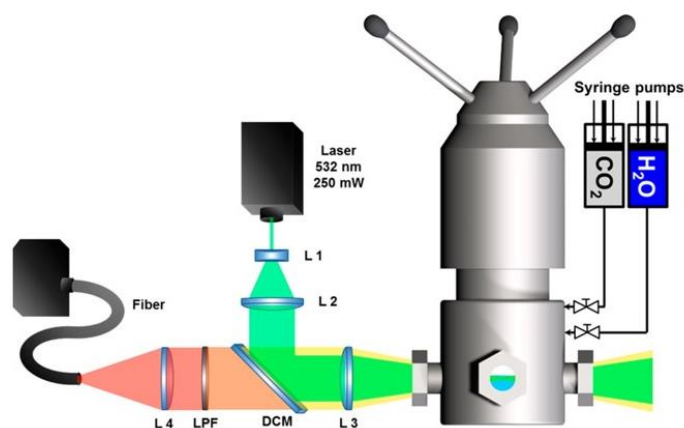
Figure 4.3 Experimental setup consisting of the high-pressure cell and the optical setup [20]

For excitation a frequency-doubled Nd: YAG laser type 532-250-AC from CNI with a wavelength of 532 nm and a power output of 250 mW was used. The beam is widened and collimated by a concave and a convex lens (L1 and L2). After that, the beam hits a dichroitic mirror (DCM) that reflects light with wavelengths shorter than 532 nm($\lambda_{reflected} < 532\ nm$) and transmits light with wavelengths longer than 544 nm($\lambda_{transmitted} > 532\ nm$). Therefore, the excitation radiation is reflected and guided through a convex lens (L 3) that focuses the laser beam into the sample cell. Inside the cell, the incident light is scattered elastically and inelastically. The inelastically scattered Raman signals are detected in backscattering direction. The scattered light is collimated by the convex lens L3 and transmitted by the dichroitic mirror.

Additionally, to the dichroitic mirror a long-pass filter (LPF) is placed in the optical path to remove the remaining elastically scattered light that was transmitted through the dichroitic mirror. Subsequently, the signals are launched into an optical fiber and guided to the spectrometer QE65Pro from Ocean Optics. Finally, a complete Raman spectrum, which it is unique for every single element, is obtained [20].

4.3. Procedure

a. Initial experiments at normal pressure

The first experiments (pure samples) were in a cuvette instead of the cell. Pure water and the inhibitors by their own were measured to produce the pure spectra. These experiments were done at atmospheric pressure and 22°C. The software that was used to display the spectra was OceanView. With this software, it is possible to configure the graph and avoid the noise of unwanted elements just recording the background before starting the measurements.

After that, the optimal solutions between the inhibitor and the water were prepared and compared [11, 53-57]. The same procedure at it was explained before was followed and the text files were processed with Matlab.

b. Experiments at 6 MPa

The experiments at high pressure take place 1n the cell explained in section 4.2. First, the cell was cleaned and flushed with water two times, and the refrigerant was set to 13 °C. For introducing the mixtures, the manual connection was used with the

help of a syringe. The cell was not completely full in order to watch the surface through the windows. Then all the connections were closed except the CO_2 pump connection and the cell pressurized with CO_2 to 6 MPa. Mixing time usually takes approximately two hours until the equilibrium CO_2-water is completed.

After this step, the temperature decreases constantly (3°C per hour) to form the hydrates. Generally, hydrates formation at these conditions occurs at temperature below 10°C so set point temperature is configured at 1°C. To analyze the kinetic of the inhibitors, the mixture stays between 3 to 5 hours at 1°C. Once the hydrate formation starts, a hydrate film is formed at the meniscus between the two liquid phases and the formation spreads and develops through the sample (figure 4.4). During the cooling and isothermal period, the fluids inside the cell were monitored with a camera and the corresponding snapshots, which are shown in figure 4.4, were continuously recorded with a frequency of 15 fps and labeled with a time stamp.
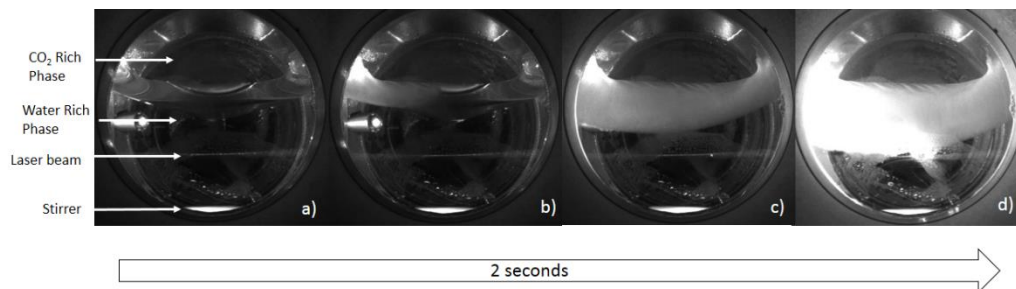
Figure 4.4 Photographs of the substances inside the cell during hydrate formation: transparent water-rich phase before hydrate formation (a), start of hydrate formation at the interface between CO_2-rich and water-rich phase (b), and further hydrate formation in the water-rich phase and development of a slurry of solid hydrate dispersed in liquid water (c, d).

To complete the measurement, the temperature was increased continuously to 13°C and suddenly to 25°C to dissociate completely the hydrate and start again the process.

Furthermore, the temperature and pressure inside the cell, the laboratory´s temperature and the refrigerant´s temperature were measured and recorded, and the Raman spectra, with an integration time of one second each, were recorded in different files.

In total, each sample repeats the cycle three times. Then the cell was depressurized and the sample was removed, in order to begin the next measurement.

c. Data Evaluation

The software OceanView give the possibility of choosing the number of scan averaged (10) and the integration time (1s). The data obtained from this software are run in Matlab. From the running of the code, the raw data are modifying. Firstly, it is obtain the spline correction in order to remove the fluorescence of the diagram. The spline correction function identifies and removes the intensity of the points inside the range of Raman shift where the intensity is supposed to be null.

Secondly, from the data resulting from the spline correction, the spectrum is normalized to the maximum. This is done in order to dismiss the different sensibility that the spectroscope has depending on the sample. Finally, the normalized spectrum is decomposed into five Gaussian peaks to quantify the R-value, which has been explained in section 3.3.3.

5. Results and Discussion

5.1. Raman Spectra of pure inhibitors and solutions

The first type of experiments (pure inhibitors) were measured in a cuvette at 22 °C (room temperature) and 1 atm. The spectrum provides the results, as shown in figure 5.1.

Most of the spectra cannot be shown because the spectrometer was saturated. For that reason, it was impossible to back up the conclusion from them.

The other three diagrams can be evaluated. Luvicap Bio has more fluorescence because of 2-butoxyethanol. This is also proven by the saturated spectra of the three HI-M-PACT inhibitors. For the three of them there is the same component, 2-butoxyethanol, and the only differences between them are the solvents and that HI-M-PACT 85232 HCW has a low concentration of quaternary ammonium compounds.
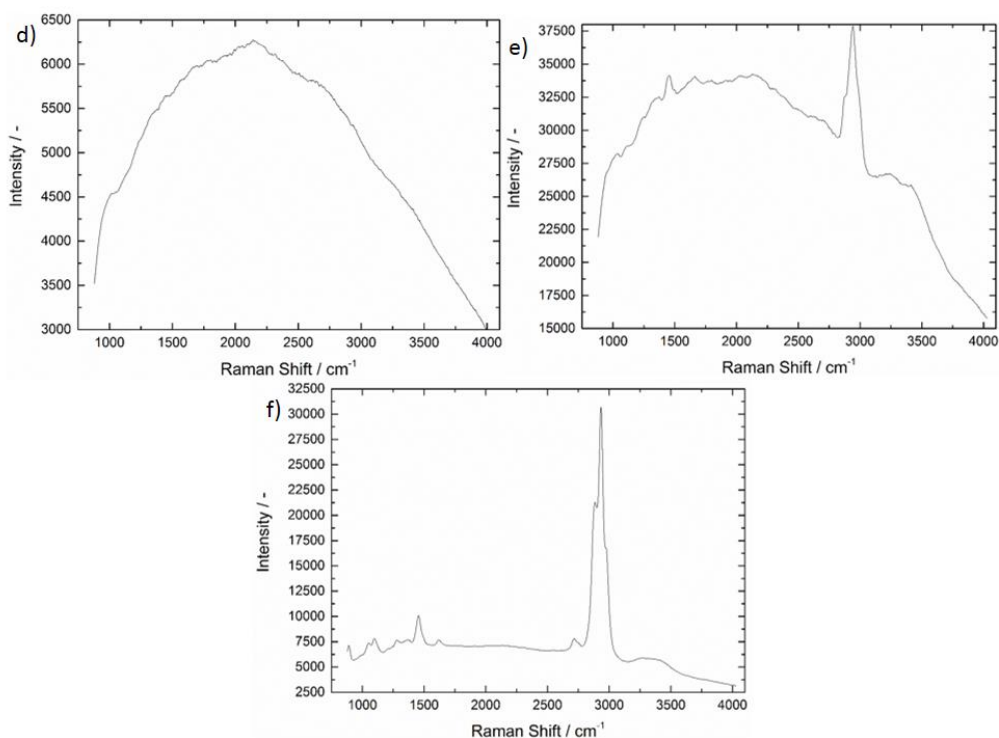
Figure 5.1 Raw Raman spectra from kinetic hydrate inhibitors tested with a green laser: Luvicap BIO (d), Luvicap 55W (e) and Luvicap PL (f)

Some similarities between Luvicap PL, Luvicap 55W and their solvents can be observe in figure 5.1. Luvicap PL (f) is dissolved in ethanol while Luvicap 55W and BIO (d and e) have water; it is easy to distinguish the O-H stretching from water and ethanol on the spectra between 3200 and 3500 cm^{-1}. In addition, the main peak is related to the C-H stretching due to the polymeric chains.

The pure inhibitors were tested with an infrared (IR) laser, because of the lack of results with the green laser. The spectra obtained are shown in figure 5.2:
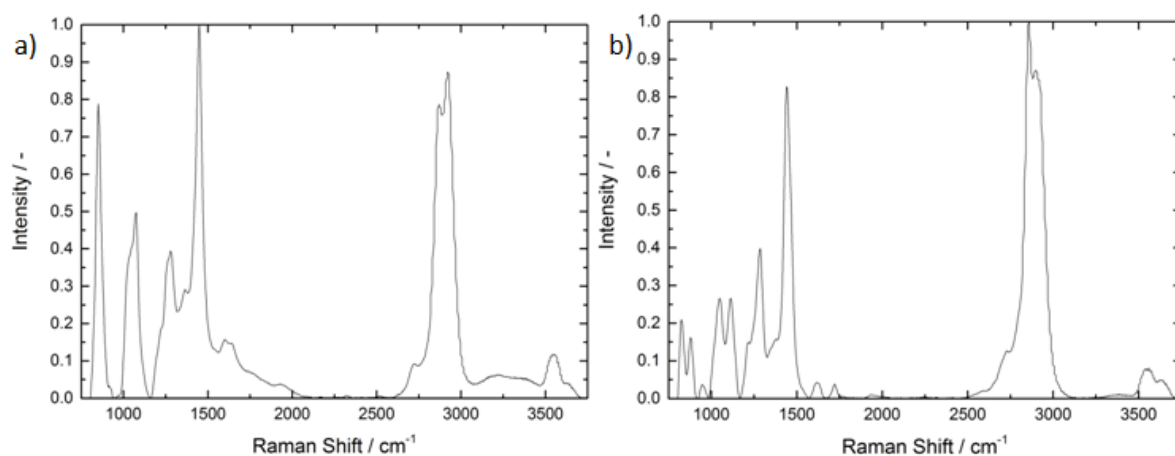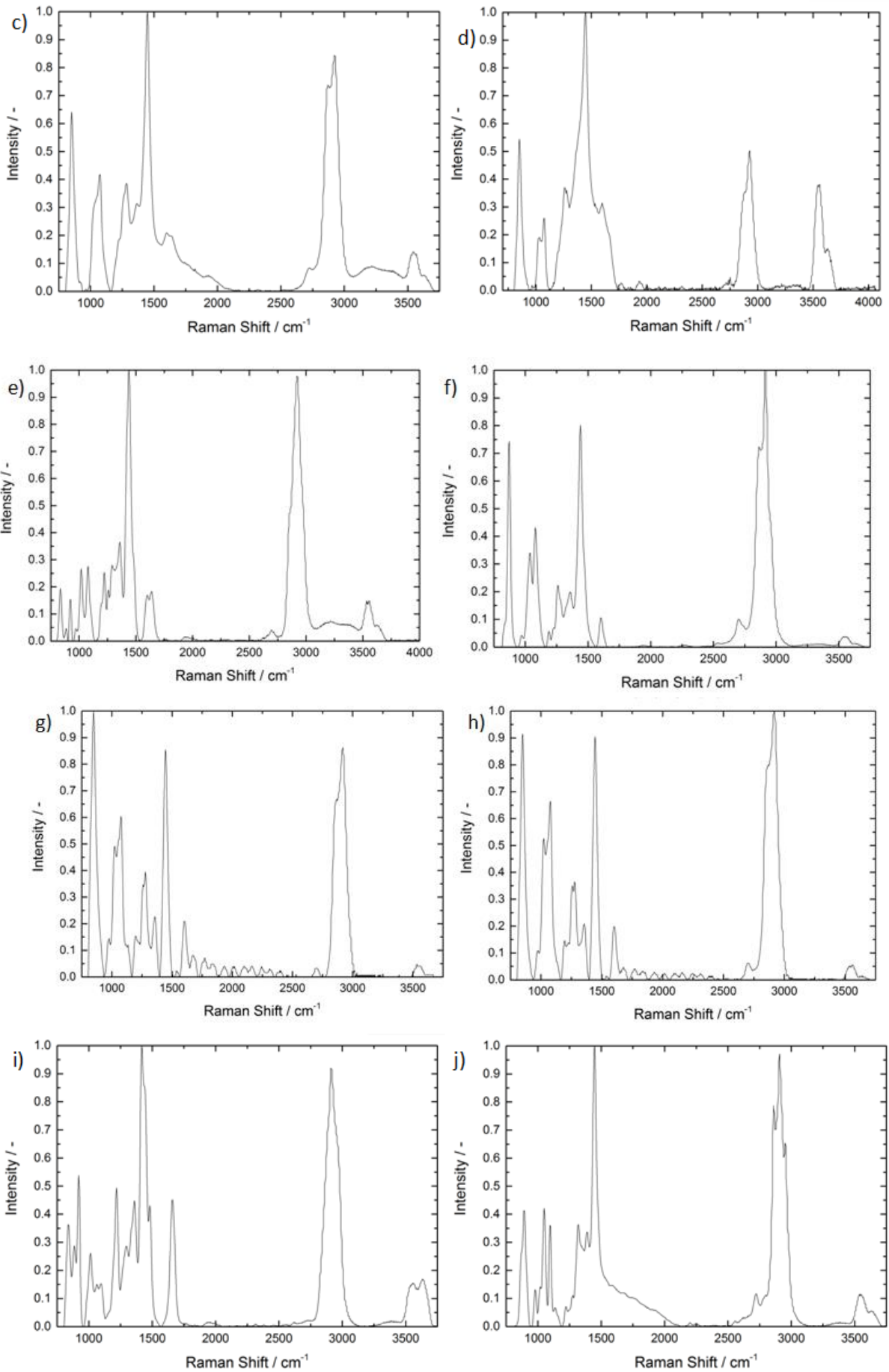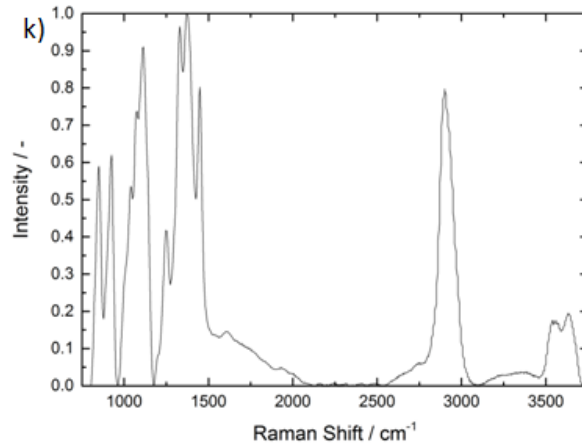
Figure 5.2 Normalized Raman spectra from kinetic hydrate inhibitors tested with an IR laser: HI-M-PACT HIW 85671 (a), HI-M-PACT HIW 85610 (b), HI-M-PACT 85232 HCW (c), Luvicap Bio (d), Luvicap 55 W (e), Luvicap PL (f), Luvicap EG (g), Luvicap EG HM (h), PVP (i), TBAB (j), Starch (k)

The inhibitor spectra show that along the range where the water stretching is located, the signal in most of the inhibitors is low. This means that the inhibitors would not influence the following measurements with the mixtures inhibitor-water and consequently, the measurements can be completed without problems. However, some of them have a weak O-H stretching signal so they were tested the solutions verify the influence on the spectrum.

Then, the mixtures of inhibitor and water were prepared and measured in a cuvette at the same conditions as the pure inhibitors (T= 22 °C; p=1 atm). Figure 5.3 and 5.4 show the comparison of the multiple normalized spectra and some detail for a better view.
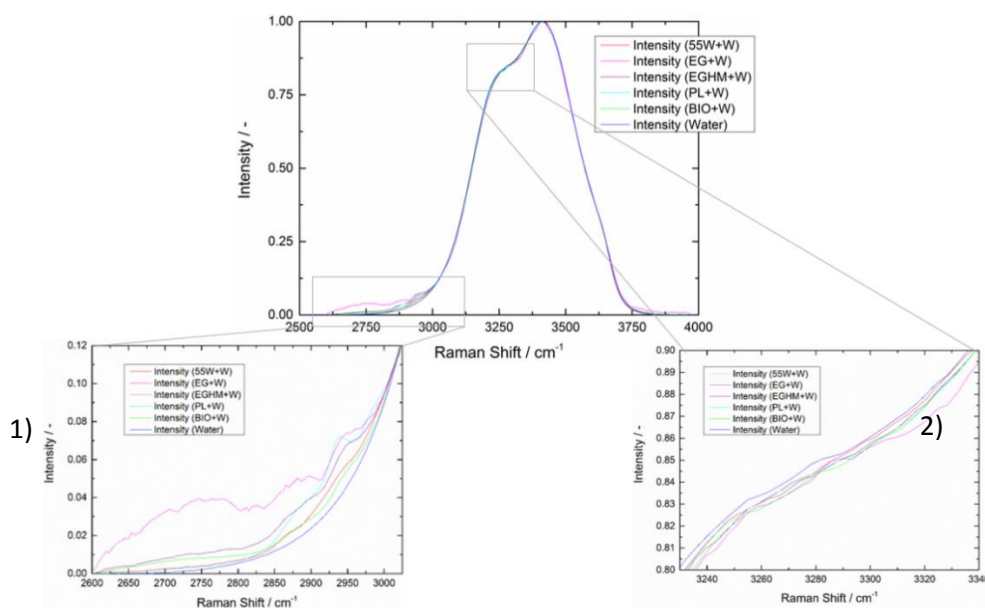
Figure 5.3 Normalized spectra comparison of the mixture between Luvicap inhibitors with water, 1) shows a magnification between the Raman Shift 2600 and 3100 cm^{-1} and 2) shows a magnification between the Raman Shift 3230 and 3340 (Isosbestic Point)
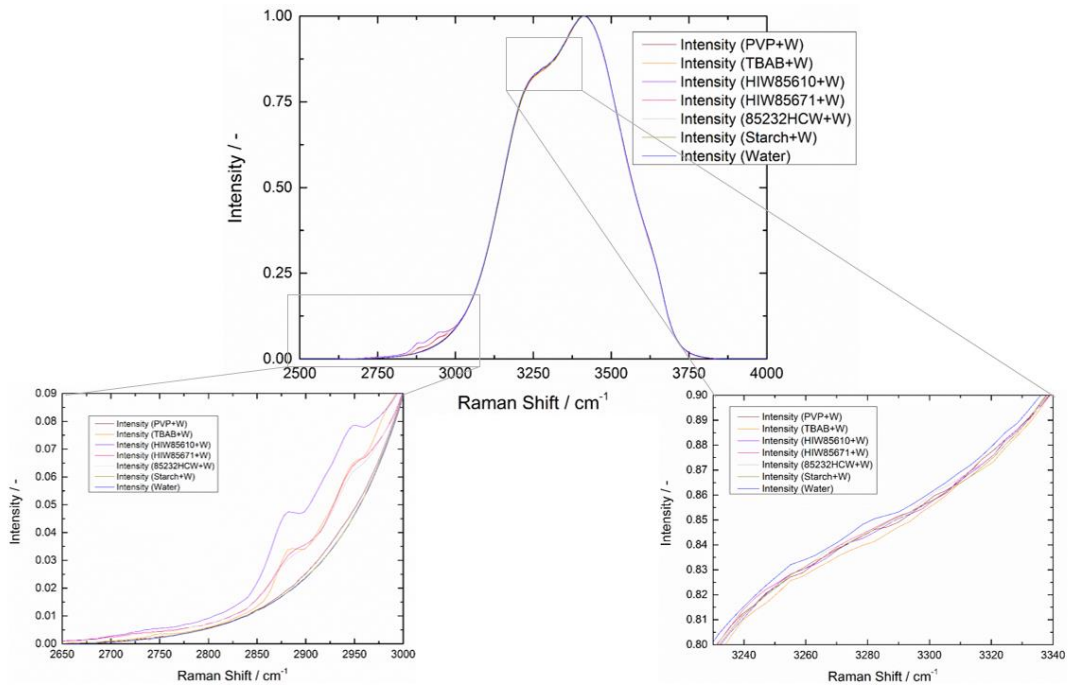
Figure 5.4 Normalized spectra comparison of the mixture between solids or HI-M-PACT inhibitors with water, 1) shows a magnification between the Raman Shift 2600 and 3100 cm^{-1} and 2) shows a magnification between the Raman Shift 3230 and 3340 (Isosbestic Point)

From these figures, the result that can be obtained is that there are no visual differences between the spectra of the pure water and the one of the mixtures. This is because the kinetic inhibitors have no influence on the hydrogen bonds. This can be demonstrated with the comparison of the R-value and the isosbestic point relation (IPR) as in figure 5.5 and 5.6. The R and the IPR-values of the pure water only defer a few hundredths from the mixture values.
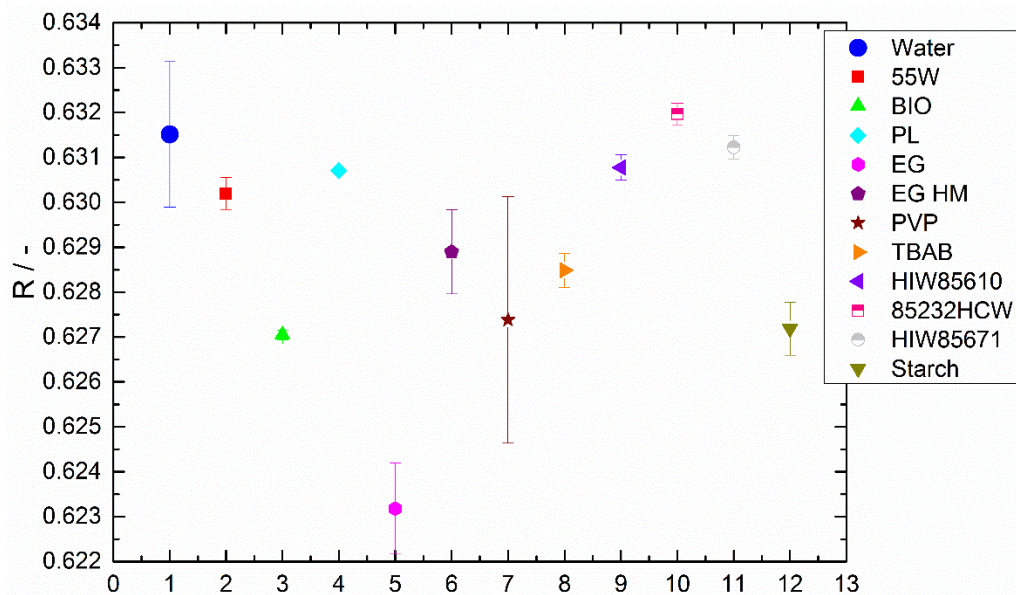
Figure 5.5 R comparisons between deionized water and samples with water and kinetics inhibitors
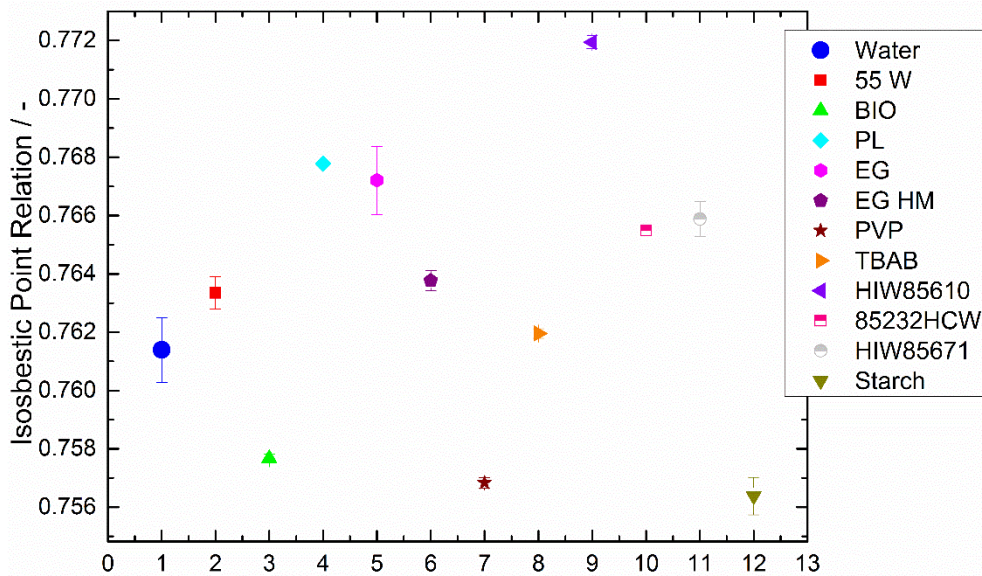
Figure 5.6 IPR comparisons between deionized water and samples with water and kinetics inhibitors

5.2. Experiments at 6 MPa

The second type of experiments was performed at high pressure (6 MPa). The samples that were used and their properties are shown in table 5.1.

N° measurement	Components	Inhibitor weight percent
1	Water	0 wt. %
2	Water + Luvicap PL	0.6 wt. %
3	Water + Luvicap 55W	0.65 wt. %
4	Water + Luvicap PL	1 wt. %
5	Water + HI-M-PACT 85232 HCW	1.03 wt. %

Table 5.1 Properties of the samples that were measured at high pressure

Each measurement consists of three cycles or repetitions that will be classified with an A, B or C.

In these experiments, the temperature inside the cell, the R and IRP-value, CO_2 concentration in water and the maximal intensity of the spectrum were measured along the time. To short the section, the representation of IRP-value is not going to be represented because it has the same tendency as the R-value.

Firstly and for a better explanation, the writer is going to describe the changes of these parameters when the sample is deionized water. Secondly, the writer is going to describe the samples water-inhibitors and to compare them with the water sample.

To see all the results and graphs of the different measurements, see *Appendix C. Measurements*.

a. Water + CO_2

The graphs correspond with one cycle of the measurement and can be divided into three sections: constant cooling (indicated with the number 1), isothermal period (indicated with the number 2) and constant heating (indicated with the number 3).

In figure 5.7 (a) and (b) are plotted some of the parameters that give some explanation about what happen to a sample with water and CO_2. Figure 5.7 (a) displays the maximum intensity and the temperature over the experimental time while figure 5.7 (b) displays the R-value and the CO_2 concentration in water over the temperature.
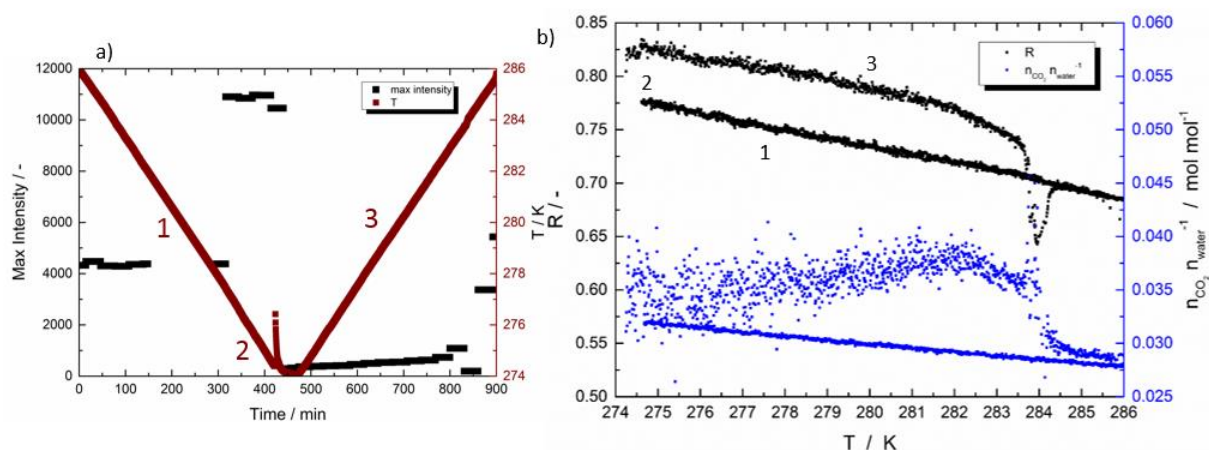
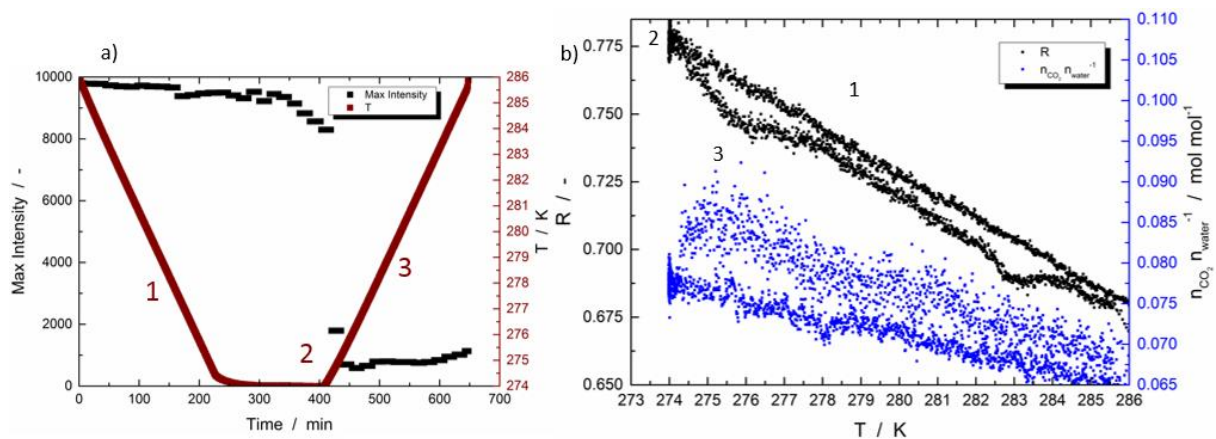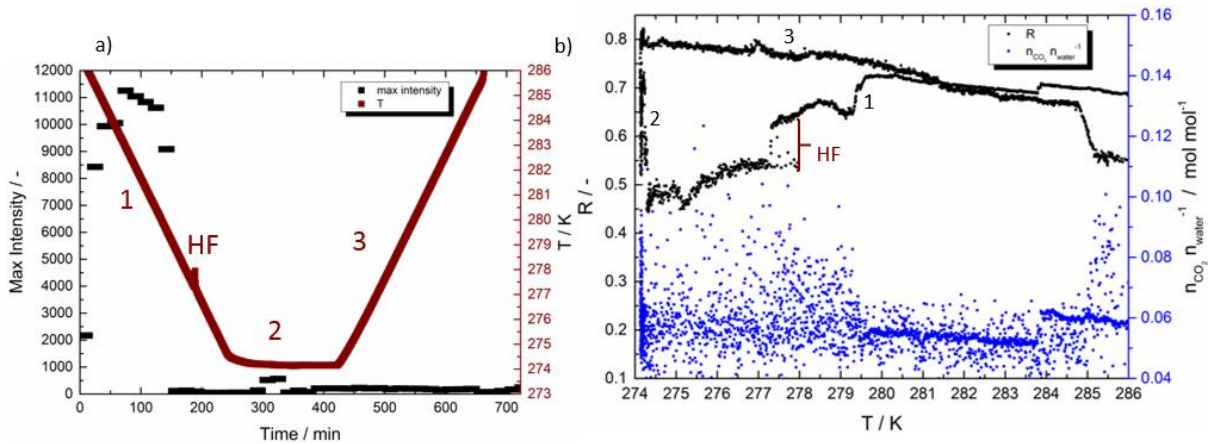*Figure 5.7 Behavior of the measured parameters when the sample is deionized water and CO_2. (Measurement 1B). Temperature inside the cell and the maximal intensity of the spectrum versus the time (a) CO_2 concentration in water and R-value versus temperature inside the cell (b)*

It is remarkable that in figure 5.7 (a) when the temperature is approximately 1ºC, the temperature instantaneously increases, between one or two degrees, and the maximal intensity drops until a minimum value (point 2). This is typical when the gas hydrate formation takes place.

Focusing now on figure 5.7 (b), it is possible to describe the effects of the gas hydrate formation on the R-value and the CO_2 concentration in water. During the cooling, the R-value increases linearly. When the temperature is near 1ºC, the R-value suffers an increment due to the gas hydrate formation. Finally, along the heating period, the R-value decreases and during the gas hydrate dissociation, the

R-value drops until a minimum value (R=0.65) and finally, it reaches the original value.

The concentration of CO_2 in water increases linearly during the cooling. When the gas hydrate instantaneously forms, the CO_2 concentration in water increases, but has not a single value instead, it is a diffusive range. Finally, along the third period (constant heating), the gas hydrate dissociates and the cycle starts again.
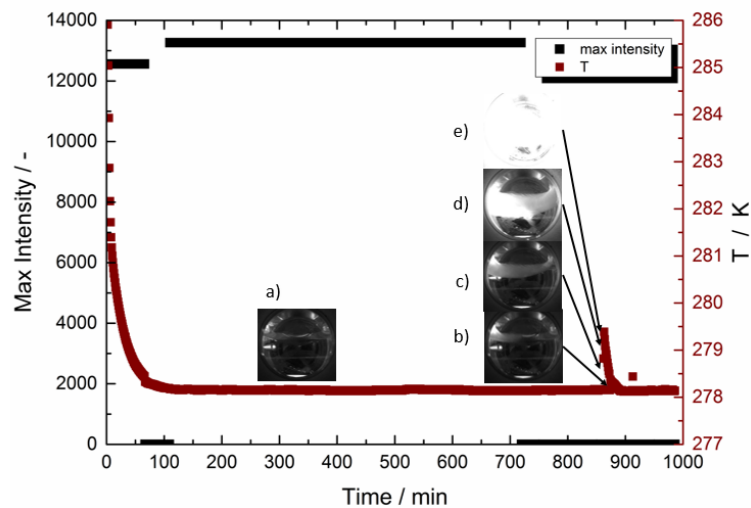
Figure 5.8 Detail of gas hydrate formation when the sample is water and CO₂ (Measurement 1A).Picture of the cell when the gas hydrate has not formed (a) Pictures of the cell while the gas hydrate formation takes place (b-e)

Figure 5.8 shows how the gas hydrate formation takes place and give some information about the characteristic of the gas hydrates formation reaction:

1) The reaction is fast. It takes place in a few seconds.
2) The reaction appears during the first or second period.
3) The reaction begins at the surface of the water-rich phase.
4) R-value increases.
5) The reaction is exothermic.
6) Maximal intensity decreases.
7) During the formation, the CO_2 is trapped by the hydrate structure and consequently, the concentration increases.

b. Water + Inhibitor + CO_2

During the following measurements, the gas hydrate formation did not appear:

- Water+ Luvicap PL(0.6 wt. %) + CO_2 (Measurement 2 A)
- Water + Luvicap 55 W (0.65 wt. %) + CO_2 (Measurement 3 A, B and C)

- Water + HI-M-PACT 85232 HCW (1.03 wt. %) + CO_2 (Measurement 5 A, B and C)

Comparing with the graphs of the mixture water-CO_2, the R-value and the temperature suffer remarkable changes as it is shown in figure 5.9. The first difference is that the peak related to the increment of temperature does not appear. This means that during the cooling and isothermal period, the gas hydrate does not form and consequently, the R-value follows a linear tendency (remember that in figure 5.7, the R-value increases during point 2 and 3).
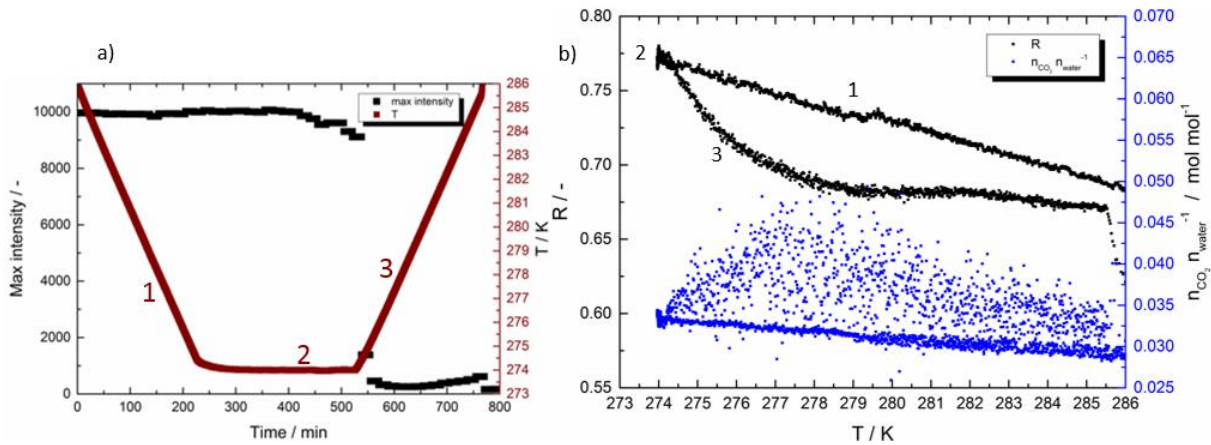
Figure 5.9 Behavior of the measured parameters when the sample is deionized water, Luvicap 55 W and CO_2. (Measurement 3 B). Temperature inside the cell and the maximal intensity of the spectrum versus the time (a) CO_2 concentration in water and R-value versus temperature inside the cell (b)

Then, when the temperature starts to increase and reaches 2°C, the maximal intensity decreases and a reaction, which will be called the "kinetic-hydrate reaction" and is shown in detail in figure 5.10, begins. The characteristics of this reaction are:

1) The reaction is slow. It takes some minutes to complete.
2) The reaction appears at the third period.
3) The reaction can begin at any point of the rich-water phase.
4) R-value decreases.
5) No temperature rise can be observed. Perhaps, the reaction is exothermic but the increment of temperature goes slowly and little by little and that is why it cannot be measured.
6) Maximal intensity decreases.
7) During the formation, the CO_2 is trapped by the hydrate structure and consequently, the concentration increases.
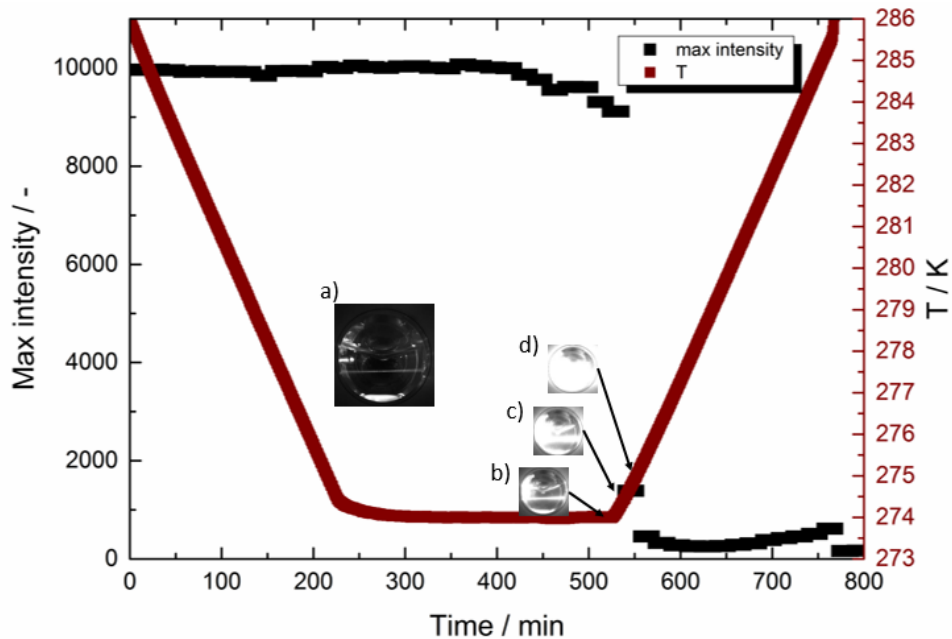
Figure 5.10 Detail of gas hydrate formation when the sample is water, Luvicap 55 W and CO₂ (Measurement 3 B) Picture of the cell when the gas hydrate has not formed (a). Pictures of the cell while the kinetic-hydrate reaction takes place (b-d)

As it is observed in the pictures from (b) to (d) in figure 5.10 and the above-mentioned characteristics, the reactions have many differences (from 1 to 4) and some similarities (6 and 7).

The behavior for the R-value during the cooling and isothermal period is predictable because the gas hydrate does not form and consequently, the R-value increases while the temperature decreases and stays at the same point when the temperature is constant. While the gas hydrate formation is spreading, the R-value decreases until a minimum (approximately 7ºC), then the dissociation begins and the R-value increases.

The CO_2 concentrations in water suffer the opposite behavior. The concentration of CO_2 in water increases linearly during the cooling. When the gas hydrate instantaneously forms, the CO_2 concentration in water increases, but has not a single value instead, it is a diffusive range. Finally, along the third period (constant heating), the gas hydrate dissociates and the cycle starts again. The only difference with the mixture water-CO_2 is that the maximum concentration is at a lower temperature, so the gas hydrate dissociation starts earlier.

The writer suggest one explanation for the behavior of the mixture and the kinetic-hydrate reaction. The polymeric chains, and particularly the active groups (amines),

interfere with the nucleus during the cooling and isothermal periods, but when the temperature increases, the hydrate growth begins, which is also indicated because the CO_2 concentration in water increases, but due to the kinetic inhibitor, the reaction is slower and because of that, the increment of temperature cannot be observed. The interaction between the polymeric chains and the nuclei is strong and deactivate the hydrate molecules. This explains why the R-value drops. When these interactions disappear when the dissociation begins, the R-value increases to the original values.

In the case of HI-M-PACT 85232 HCW, the graphs in figure 5.11 show that is less effective than the other measured inhibitor. Largely because the R-value is increasing and decreasing linearly and does not suffer high variation and the CO_2 concentration is higher (0.08) (remember that in figure 5.9 the maximum was at 0.045). This means, that the interaction are not as strong as the other inhibitor.

Figure 5.11 Behavior of the measured parameters when the sample is deionized water, HI-M-PACT 85232 HCW and CO_2. (Measurement 5 C). Temperature inside the cell and the maximal intensity of the spectrum versus the time (a) CO_2 concentration in water and R-value versus temperature inside the cell (b)

Nevertheless, the inhibitors are not always effective. This appears when the sample contains an inhibitor but it does not work and the gas hydrate forms. This case happened in the following measurements:

- Water+ Luvicap PL(0.6 wt. %) + CO_2 (Measurement 2 A)
- Water + Luvicap PL (1 wt. %) + CO_2 (Measurement 4 A, B and C)

Figure 5.12 Behavior of the measured parameters when the sample is deionized water, Luvicap PL and CO_2. (Measurement 4 A). Temperature inside the cell and the maximal intensity of the spectrum versus the time (a) CO_2 concentration in water and R-value versus temperature inside the cell (b)

Figure 5.12 (a) and (b) show the formation of the gas hydrate at approximately 4 ⁰C. The properties seem to be the same as the water-CO_2 case (the temperature and de CO_2 concentration in water increase while the maximal intensity decreases) but the R-value decreases instead of reaching a higher value. After that, the R-value is still decreasing and during the isothermal period, it continuously increasing until the maximum point (R=0.81). This maximum point is a little bit lower than the mixture water-CO_2. Finally, during the heating period, the gas hydrate dissociates.
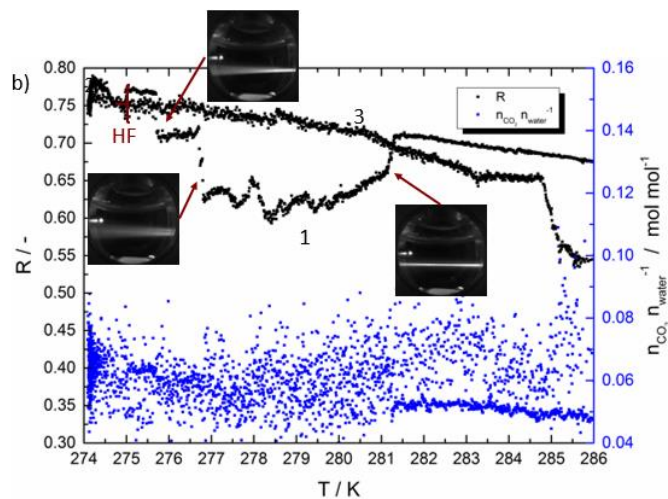
Figure 5.13 CO_2 concentrations in water and R-value versus temperature inside the cell (Measurement 4 B). Picture of the cell during the cooling period when the temperature is 8.12 ⁰C (a) Picture of the cell during the cooling period when the temperature is 3.65 ⁰C (b) Picture of the cell during the cooling period when the temperature is 2.57 ⁰C (c)

It is also remarkable that during the cooling period, the R-value suffers some fallings and increments. Figure 5.13 reveals that during the increments of R-value the light beam is not focus, but during the decrements, the laser beam is focalized in the sample.
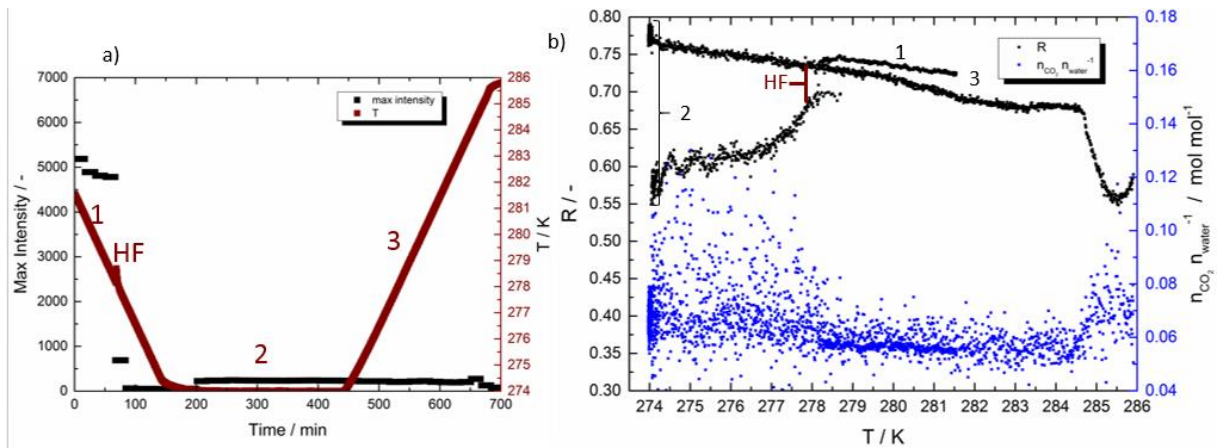
Figure 5.14 Behavior of the measured parameters when the sample is deionized water, Luvicap PL and CO_2.(Measurement 4 C) Temperature inside the cell and the maximal intensity of the spectrum versus the time (a) CO_2 concentration in water and R-value versus temperature inside the cell (b)

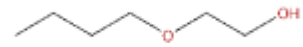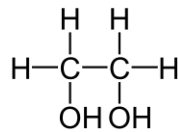During the third cycle of measurement 5, another significant event takes places as is shown in figure 5.14. Along the isothermal section, the R-value increases instantaneously from the minimum point (R=0.55) to the maximum (R=0.8).

6. Conclusion

In this work, a variety of KHIs had been tested for gas hydrate inhibition using Raman spectroscopy. The following conclusions can be drawn from the results that have been obtained.

From the first type of experiments at atmospheric pressure can conclude that KHIs do not shift the equilibrium to WHB and SHB water molecules at normal conditions. As it is known, just thermodynamic inhibitors shift the equilibrium.

Secondly, and focusing on the second type of experiments, more conclusions can be drawn. When KHIs inhibit the hydrate formation, they have an influence on the R-value because of the interferences of the polymeric chains in the gas hydrate structure.

The concentration of KHI has an influence, as it was shown during the measurements of Luvicap PL at the optimal concentration (0.6 wt. %) and the maximum concentration for KHI (1 wt. %). When the inhibitors are not at the optimal concentration, it does not inhibit the gas hydrate formation as it happens with Luvicap PL at 1 wt. %.

Although, Luvicap PL shows some problems during measurement 3 A because did not inhibit gas hydrate formation at the optimal concentration. Just in measurement 3 C, the inhibitor works properly. For this reason, it could be possible that the sample was not in good conditions and perhaps the inhibitor was degraded during the storage time or during the experiment.

When the KHIs works properly, then the kinetic-hydrate reaction always takes place when the temperature is starting to rise, that means, that the temperature is between 1ºC and 2ºC. In addition, Luvicap 55 W and HI-M-PACT 85232 HCW follow the same pattern in spite of the difference of the components; this means that all the KHI works in a similar way. Nevertheless, Luvicap 55 W is more effective and ensures the mixture to stay stable because the interaction with the nuclei are stronger than with the others.

Finally and because this topic need to be investigated in more detail. More measurements should be done for a better determination of the influence of KHIs. It is also important to make some researches on how KHIs work and how can change the kinetic of the reaction. Carrying out a study about the gas hydrate formation does not start at the surface of the water rich phase can be also interesting and can give some clues about kinetics inhibitors.

Appendix A. List of Figures and Tables

A.1. List of Figures

A.2. List of Table

Appendix B. Safety Sheets

HI-M-PACT HIW 85671

Name: HI-M- PACT HIW85671

Firma: Baker Hughes

Components

1. Ethandiol (35-50wt. %)
2. 2-butoxyethanol (10-20wt. %)

Rate: It can be applied at 0.1-1 wt. % based on water production.

Safety (HA: Help Aids)

Main Hazards: Harmful. Danger of serious damage to health by prolonged exposure if swallowed

Hazardous ingredients: Ethandiol

R-phases:

- R20/21/22: Harmful by inhalation and in contact with skin
- R36/38: Irritating to eyes and skin
- R48/22: Harmful: danger of serious damage to health by prolonged exposure through inhalation.

S-phases:

- S26: In case of contact with eyes, rinse immediately with plenty of water and seek medical advice.
- S36: Wear suitable protective clothing.

Prevention:

- Wear protective gloves. Wear eye or face protection. Do not breathe vapor.

Response:

- Get medical attention if you feel unwell. If swallowed: call a poison center or physician if you feel unwell.

HI-M-PACT HIW 85610

Name: HI-M- PACT HIW85610

Firma: Baker Hughes

Components

1. 2-butoxyethanol (50-75wt. %)

Rate: It can be applied at 0.1-1 wt. % based on water production.

Safety (HA: Help Aids)

Main Hazards: Harmful. Danger of serious damage to health by prolonged exposure if swallowed

Hazardous ingredients: 2-butoxyethanol
R-phases:

- R20/21/22: Harmful by inhalation and in contact with skin
- R36/38: Irritating to eyes and skin
- R48/22: Harmful: danger of serious damage to health by prolonged exposure through inhalation.

S-phases:

- S26: In case of contact with eyes, rinse immediately with plenty of water and seek medical advice.
- S36: Wear suitable protective clothing.

Prevention:

- Wear protective gloves. Wear eye or face protection. Do not breathe vapor.

Response:

- Get medical attention if you feel unwell. If swallowed: call a poison center or physician if you feel unwell.

HI-M-PACT 85232 HCW

Name: HI-M- PACT 85232 HCW

Firma: Baker Hughes
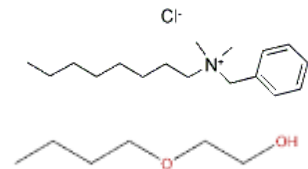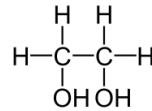
Components

1. Ethandiol (20-25 wt. %)
2. 2-butoxyethanol (10-20 wt. %)
3. Quaternary ammonium compounds, benzyl-C12-16-alkyldimethyl, chlorides (0.1-15 wt. %)

Rate: It can be applied at 0.1-1 wt. % based on water production.

Safety (HA: Help Aids)

Main Hazards: Harmful. Danger of serious damage to health by prolonged exposure if swallowed

Hazardous ingredients: Ethanediol

R-phases:

- R20/21/22: Harmful by inhalation and in contact with skin
- R34: Causes burns
- R36/38: Irritating to eyes and skin
- R48/22: Harmful: danger of serious damage to health by prolonged exposure through inhalation.
- R50: Vey toxic to aquatic organisms

S-phases:

- S26: In case of contact with eyes, rinse immediately with plenty of water and seek medical advice.
- S36: Wear suitable protective clothing.

Prevention:

- Wear protective gloves. Wear eye or face protection. Do not breathe vapor.

Response:

- Get medical attention if you feel unwell. If swallowed: call a poison center or physician if you feel unwell.

Luvicap BIO

Name: Luvicap BIO

Firma:BASF SE

Components

1. Vinylcaprolactam (VCap)
2. Water (dissolvent)
3. Mono butyl glycol ether.
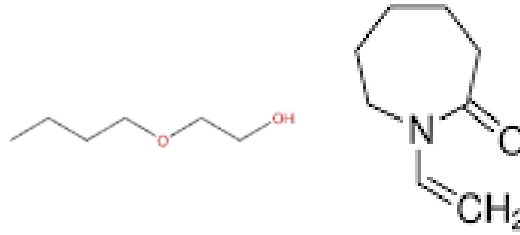
Rate: It can be applied at 0.5 wt. % to 3 wt. % based on water production.

Safety (HA: Help Aids)

Main Hazards: Harmful. Danger of serious damage to health by prolonged exposure if swallowed

Hazardous ingredients: Ethandiol
R-phases:

- R22: Harmful if swallowed
- R48/22: Harmful: danger of serious damage to health by prolonged exposure through inhalation.

S-phases:

- S2: Keep out of the reach of children
- S45: In case of accident or if you feel unwell seek medical advice immediately (sow the label where possible)

Prevention:

- Do not breathe vapor.

Response:

Luvicap 55W

Name: Luvicap 55W

Firma: BASF SE

Components

1. 1-Vinyl-2-pyrrolidone.
2. 1-vinylhexahydro-2H-azepin-2-one
3. Water (dissolvent)
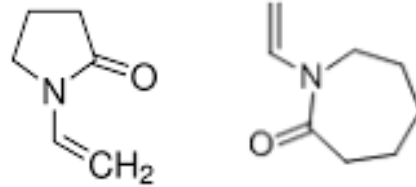
Rate: Approximately 0.4 wt. % or 4000 ppm.

Safety (HA: Help Aids)

Main Hazards: No particular hazards known if the standards are met / notes for storage and handling.

Hazardous ingredients:
R-phases:

S-phases:

Prevention:

Response:

- Immediately and rinse for at least 15 minutes holding the eyelids apart thoroughly under running water, ophthalmologist.
- Rinse mouth and drink plenty of water.
- Wash thoroughly with soap and water.

Luvicap PL

Name: Luvicap PL

Firma: BASF SE
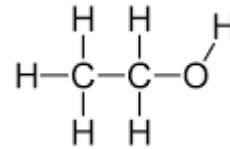
Components

1. 2H-Azepin-2-one
2. 1-ethenylhexahydro-homopolymer
3. Ethanol (dissolvent)

Rate: It can be applied at 0.5 vol% to 0.75 vol% based on water production.

Safety (HA: Help Aids)

Main Hazards: Harmful. Danger of serious damage to health by prolonged exposure if swallowed

Hazardous ingredients: Ethanol

R-phases:

- R11: Highly flammable.
- R38: Irritating to skin.
- R41: Risk of serious damage to eyes.

S-phases:

- S7: Keep container tightly closed
- S16: Keep away from sources of ignition- No smoking
- S24/25: Avoid contact with skin and eyes
- S26: In case of contact with eyes, rinse immediately with plenty of water and seek medical advice.
- S28.1: After contact with skin, wash immediately with soap and water
- S37/39: Wear suitable gloves and eye/face protection.

Prevention:

- Wear protective gloves. Wear eye or face protection.

## Luvicap EG

Name: Luvicap EG

Firma: BASF SE

Components
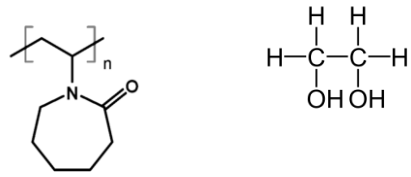
1. Polyvinylcaprolactam
2. Ethandiol (Glycol) (50-75wt. %) (dissolvent)

Rate: It can be applied at 0.5 vol. % to 3 vol. % based on water production.

Safety (HA: Help Aids)

Main Hazards: Harmful. Danger of serious damage to health by prolonged exposure if swallowed

Hazardous ingredients: Ethan-1,2-diol

R-phases:

- R22: Harmful if swallowed
- R48/22: Harmful: danger of serious damage to health by prolonged exposure through inhalation.

S-phases:

- S2: Keep out of the reach of children
- S36/37: Wear suitable protective clothing and gloves
- S45: In case of accident or if you feel unwell seek medical advice immediately (sow the label where possible)

Prevention:

- Wear protective gloves. Wear eye or face protection. Do not breathe vapor.

Response:

- Get medical attention if you feel unwell. If swallowed: call a poison center or physician if you feel unwell.

Luvicap EG-HM

Name: Luvicap EG-HM

Firma: BASF SE

Components

1. Polyvinylcaprolactam
2. Ethandiol (Glycol) (50-75wt. %) (dissolvent)
3. Quaternary ammonium compounds, benzyl-C12-16-alkyldimethyl, chlorides (0.1-15wt. %)
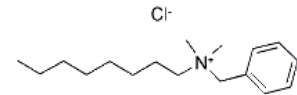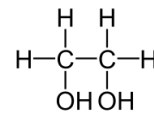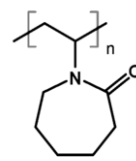
Rate: It is used just in low proportion (0.5 wt. %).

Safety (HA: Help Aids)

Main Hazards: Harmful. Danger of serious damage to health by prolonged exposure if swallowed

Hazardous ingredients: Ethan-1,2-diol
R-phases:

- R22: Harmful if swallowed
- R48/22: Harmful: danger of serious damage to health by prolonged exposure through inhalation.

S-phases:

- S2: Keep out of the reach of children
- S36/37: Wear suitable protective clothing and gloves
- S45: In case of accident or if you feel unwell seek medical advice immediately (sow the label where possible)

Prevention:

- Wear protective gloves. Wear eye or face protection. Do not breathe vapor.

Response:

- Get medical attention if you feel unwell. If swallowed: call a poison center or physician if you feel unwell.

PVP

Name: Polyvinylpyrrolidone.

Firma: Merck Millipore

Components

1. Polyvinylpyrrolidone

Rate: It is used just in low proportion (0-0.07 wt. %).

Safety (HA: Help Aids):

Hazardous ingredients: Polyvinylpyrrolidone

Prevention:

- Wear protective gloves. Wear eye or face protection.

Response:

- Eye contact: Immediately flush eyes with plenty of water for at least 15 minutes, occasionally lifting the upper and lower eyelids. Check for and remove any contact lenses. Get medical attention if irritation occurs.
- Skin contact: Flush contaminated skin with plenty of water. Remove contaminated clothing and shoes. Get medical attention if symptoms occur. Wash clothing before reuse.
- Inhalation: Move exposed person to fresh air. Keep person warm and at rest. If not breathing, if breathing is irregular or if respiratory arrest occurs, provide artificial respiration or oxygen by trained personnel. It may be dangerous to the person providing aid to give mouthto-mouth resuscitation. Get medical attention if symptoms occur.
- Ingestion: Wash out mouth with water. If material has been swallowed and the exposed person is conscious, give small quantities of water to drink. Stop if the exposed person feels sick as vomiting may be dangerous. If vomiting occurs, the head should be kept low so that vomit does not enter the lungs. Get medical attention if symptoms occur.
- Protection of first-aiders: No action shall be taken involving any personal risk or without suitable training
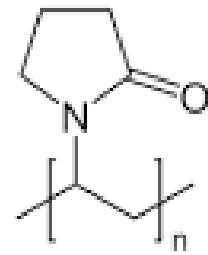
TBAB

Name: Tetrabutylammoniumbromide.

Firma: Merck

Components

1. Tetrabutylammoniumbromide (50% solution in water).

Rate: It is used just in low proportion (1 wt. %) or between 1000-5000 ppm.

Safety (HA: Help Aids):

Main Hazards: Harmful

Hazardous ingredients: Tetrabutylammoniumbromide

R-phases:
- R20: Harmful by inhalation
- R22: Harmful if swallowed
- R36: Irritating to eyes
- R37: Irritating to respiratory system
- R38: Irritating to skin

S-phases:
- S26: In case of contact with eyes, rinse immediately with plenty of water and seek medical advice.
- S36: Wear suitable protective clothing.

Prevention:
- Wear protective gloves. Wear eye or face protection. Do not breathe vapor.

Response:
- Get medical attention if you feel unwell. If swallowed: call a poison center or physician if you feel unwell.
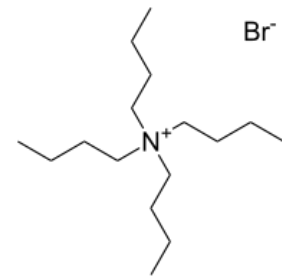
Starch, from potato

Name: Starch, from potato, soluble

Firma: Alfa Aesar GmbH & Co. KG

Components

1. Amylase
2. Amylopectin
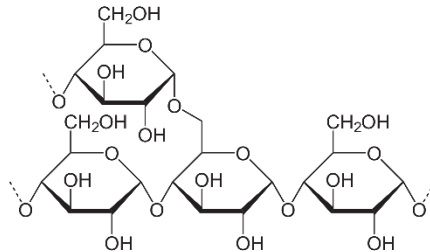
Rate: It can be applied at 0.5 wt. %

Safety (HA: Help Aids)

Main Hazards:

Hazardous ingredients:

R-phases:

S-phases:

Prevention:

- Wear protective gloves. Wear eye or face protection. Do not breathe vapor.

Response:

- Breathe in: Fresh air, if necessary give artificial respiration heat. Then consult a doctor.
- Contact with the skin: wash with water and soap.
- Contact with the eyes: Immediately and rinse for at least 15 minutes holding the eyelids apart thoroughly under running water, ophthalmologist.

Appendix C. Measurements

Measurement 1
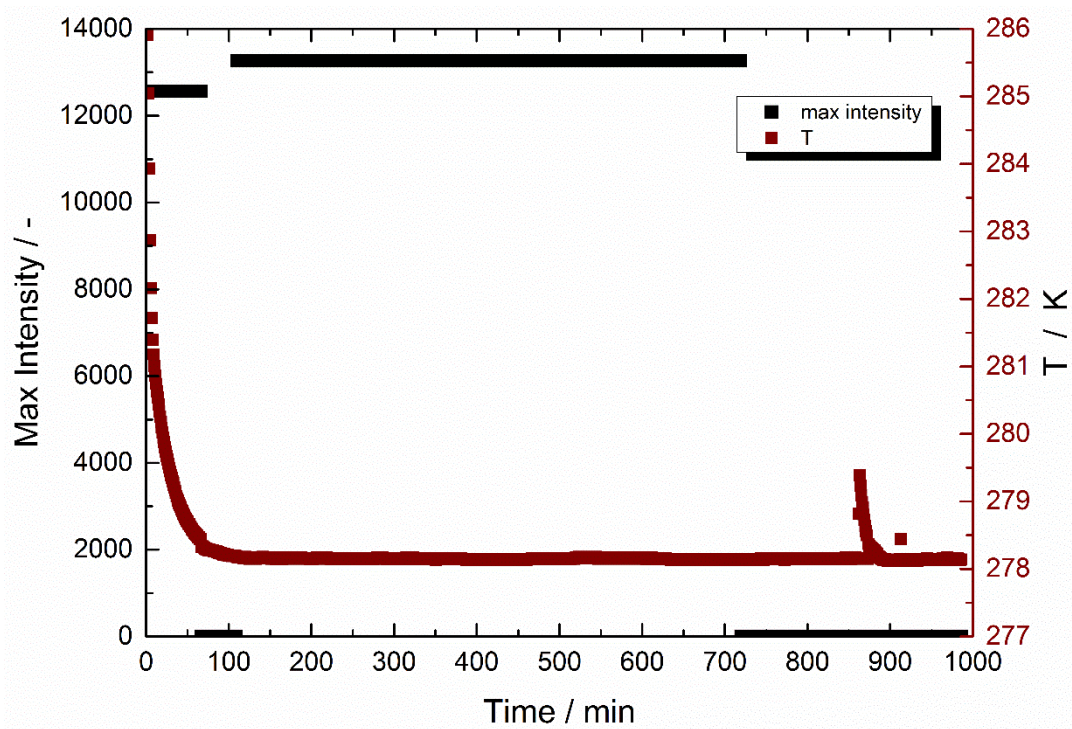
Figure C.1 Measurement 1 A(water and CO_2): Temperature inside the cell and the maximal intensity of the spectrum versus the time
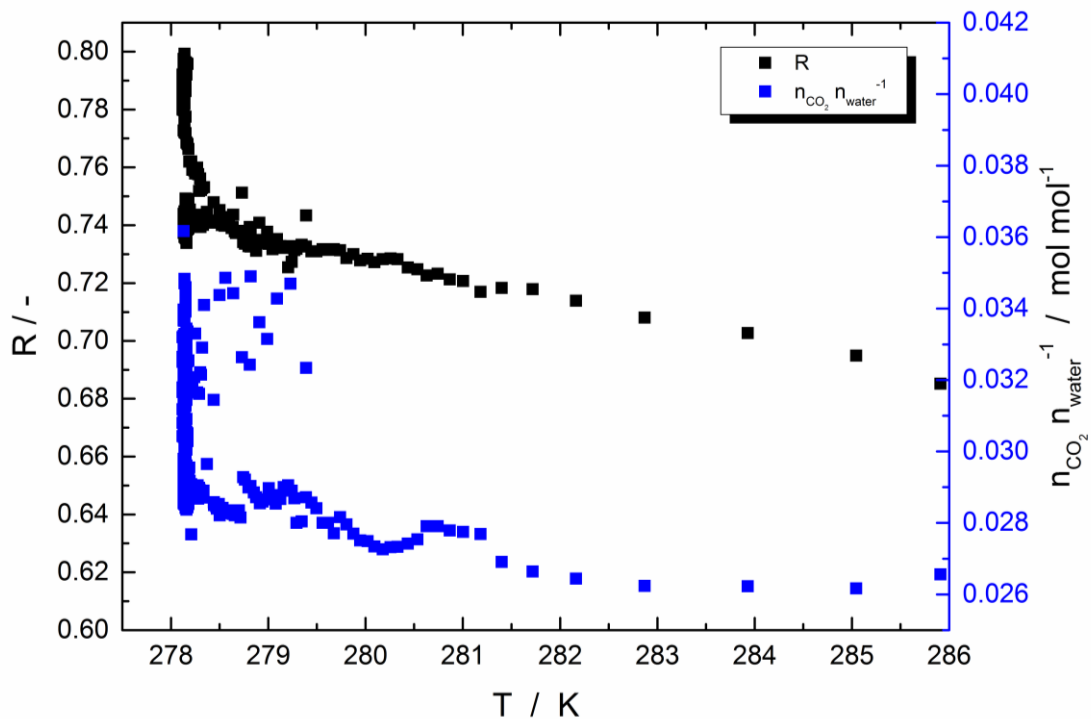
Figure C.2 Measurement 1 A (water and CO_2):CO_2 concentration in water and R-value versus temperature inside the cell
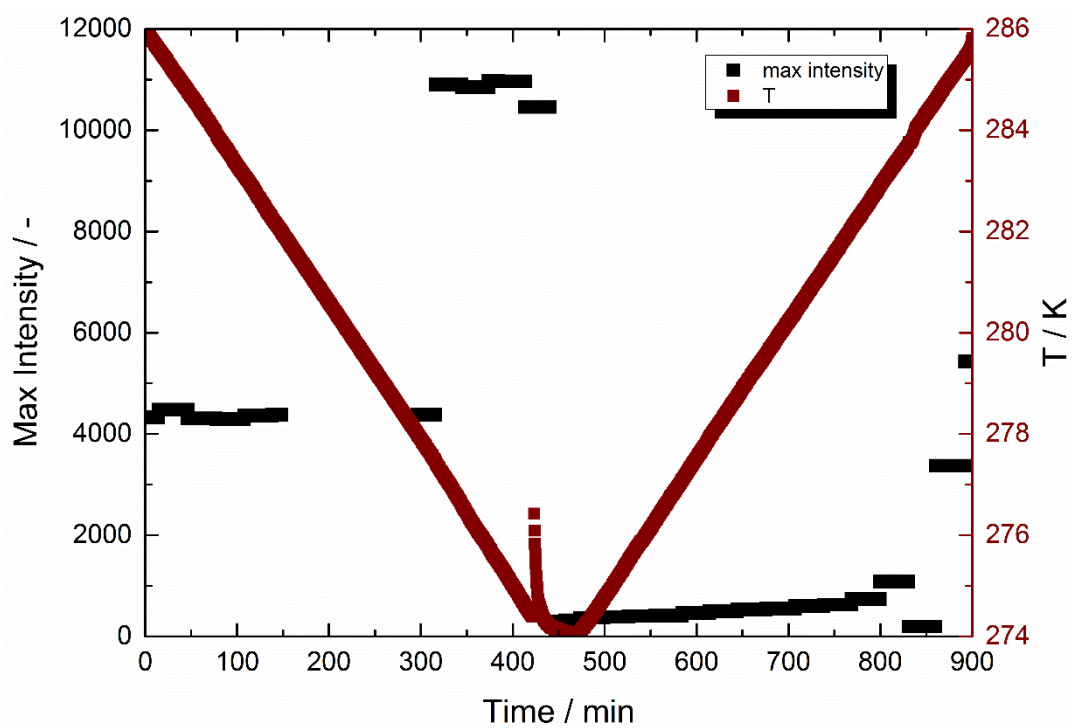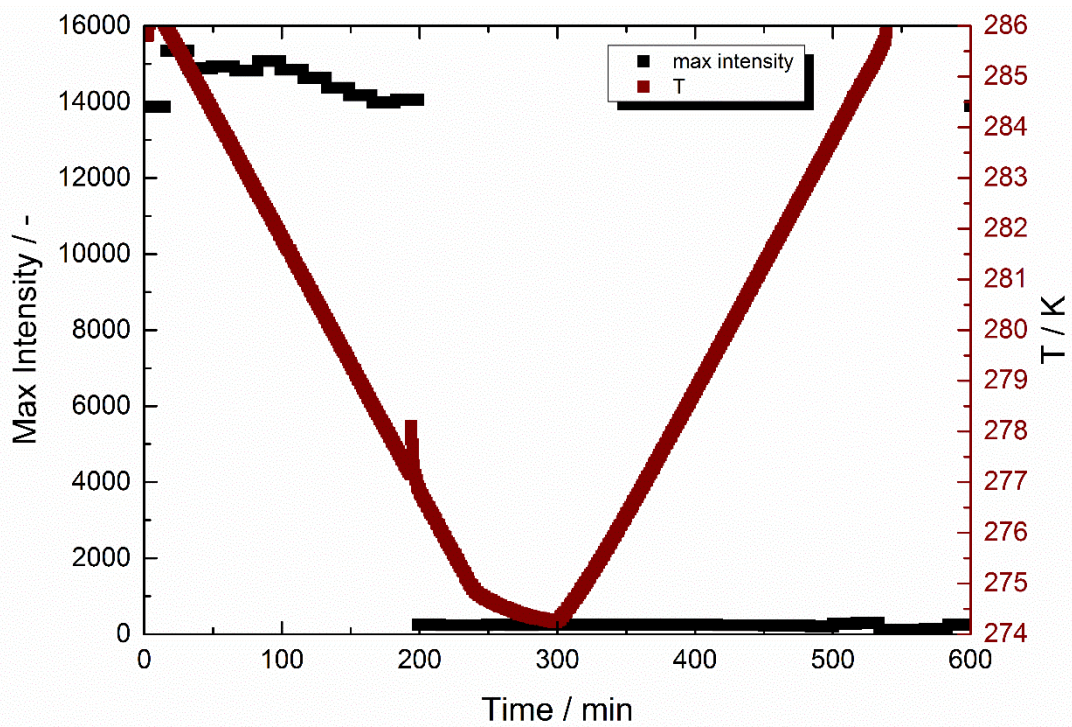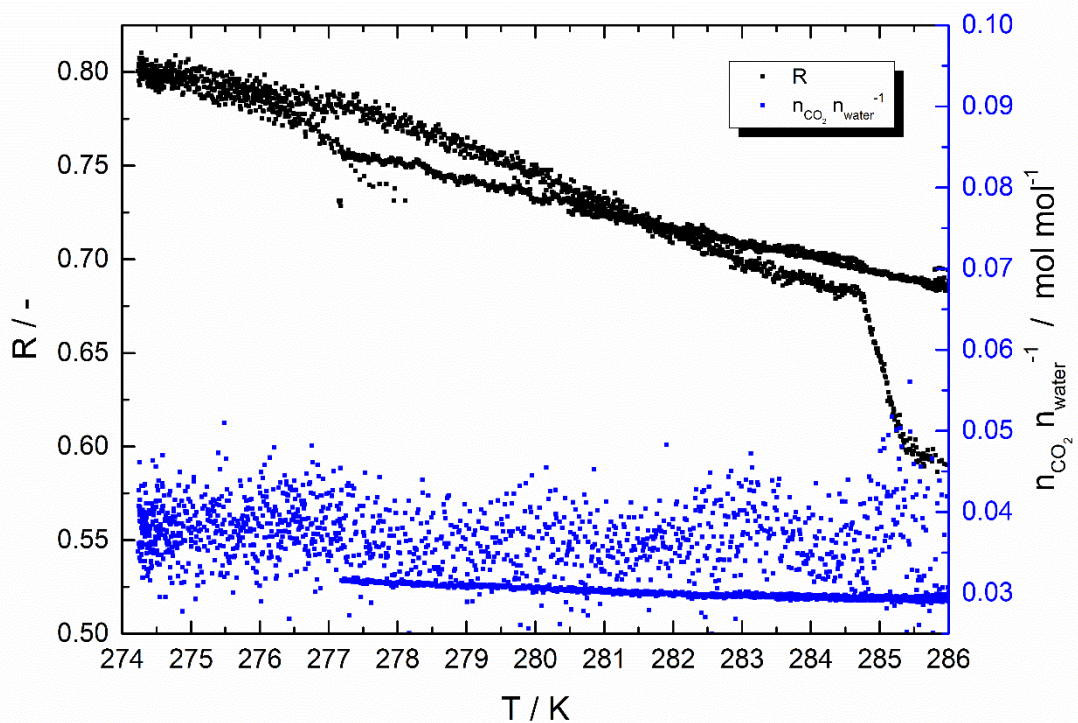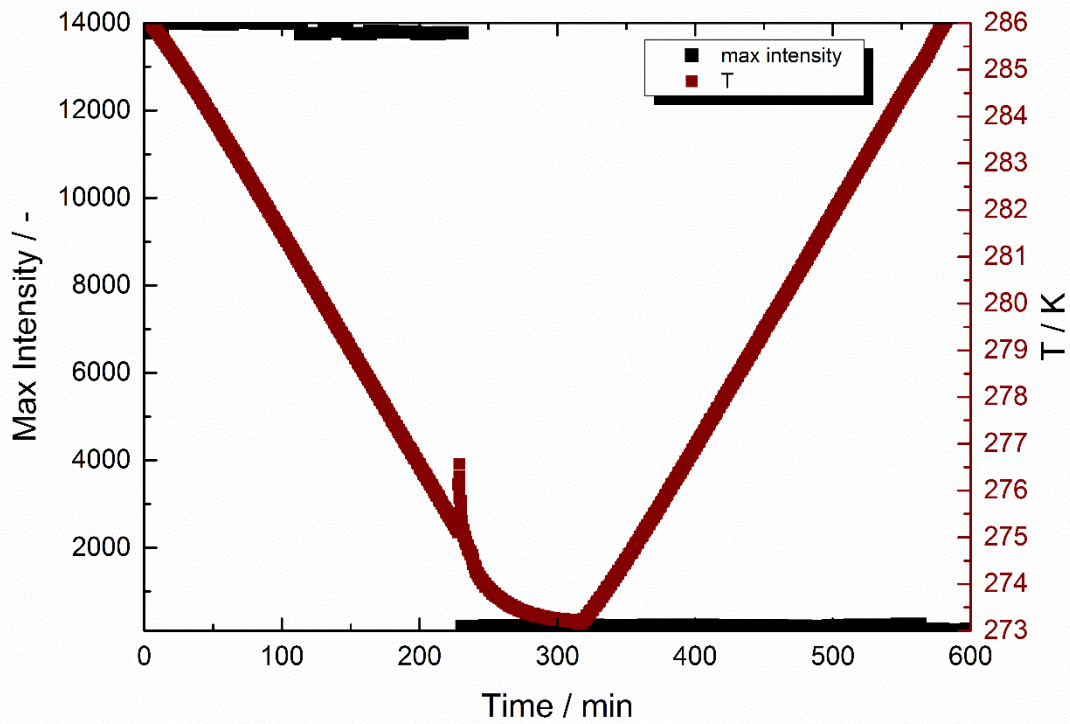
Figure C.3 Measurement 1 B (water and CO$_2$): Temperature inside the cell and the maximal intensity of the spectrum versus the time
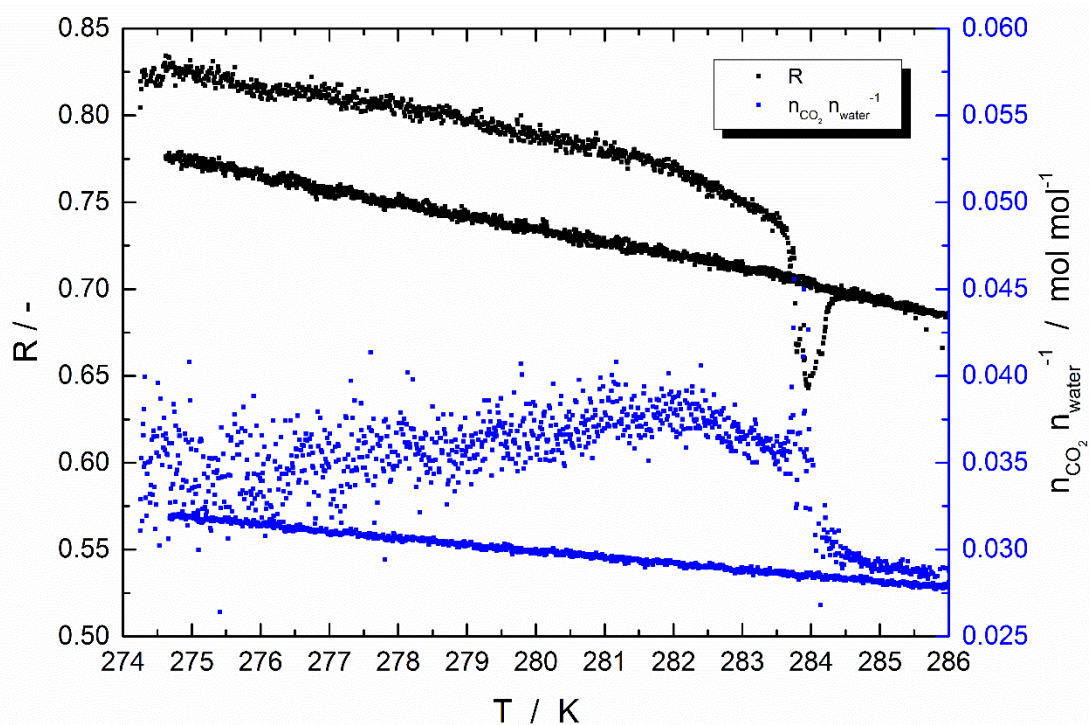
Figure C.4 Measurement 1 B (water and CO$_2$):CO$_2$ concentration in water and R-value versus temperature inside the cell

Figure C.6 Measurement 2 A (water, Luvicap PL (0.6 wt. %) and CO$_2$): Temperature inside the cell and the maximal intensity of the spectrum versus the time
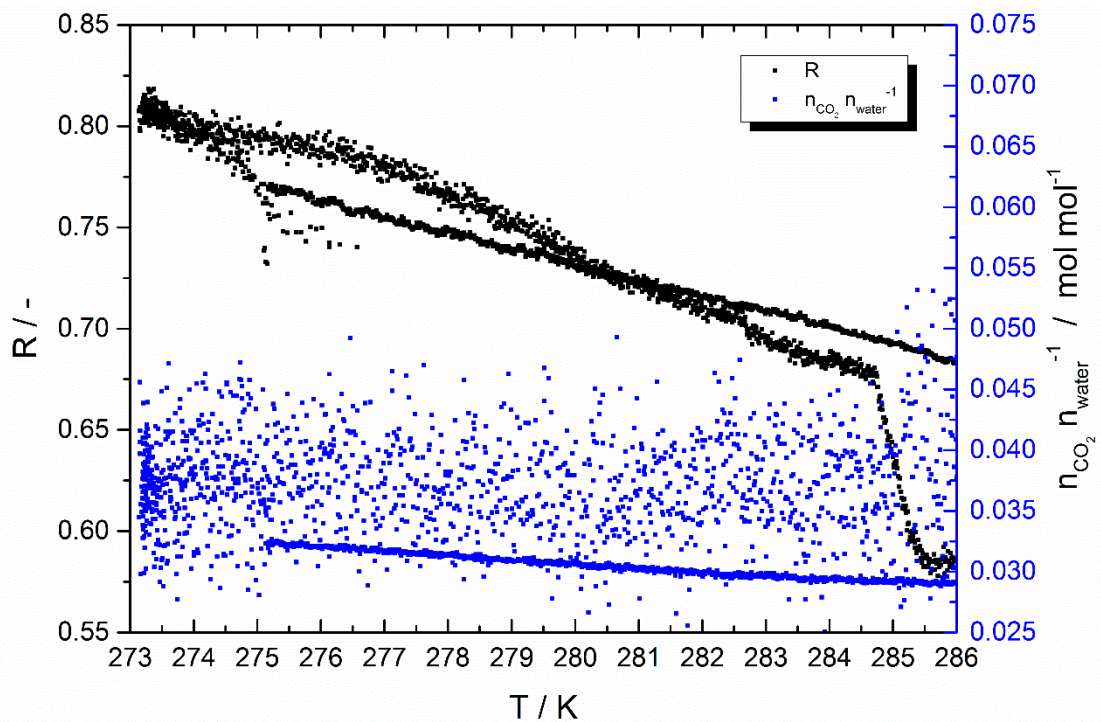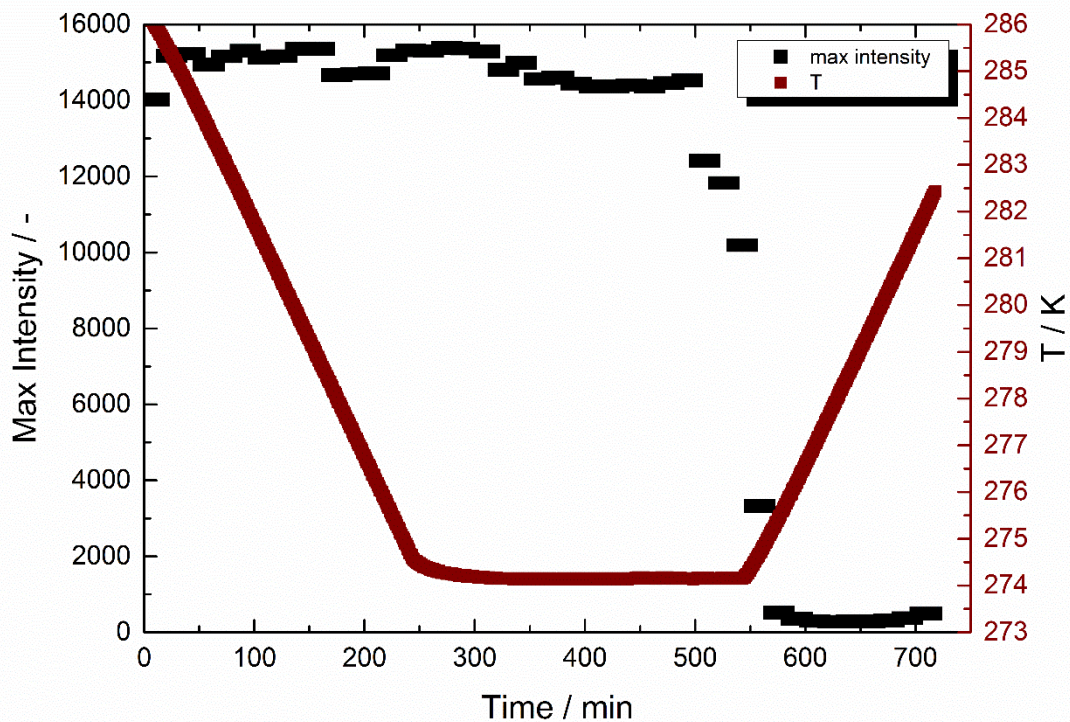

Figure C.7 Measurement 2 A (water, Luvicap PL (0.6 wt. %) and CO$_2$):CO$_2$ concentration in water and R-value versus temperature inside the cell

Figure C.8 Measurement 2 B (water, Luvicap PL (0.6 wt. %) and CO_2): Temperature inside the cell and the maximal intensity of the spectrum versus the time
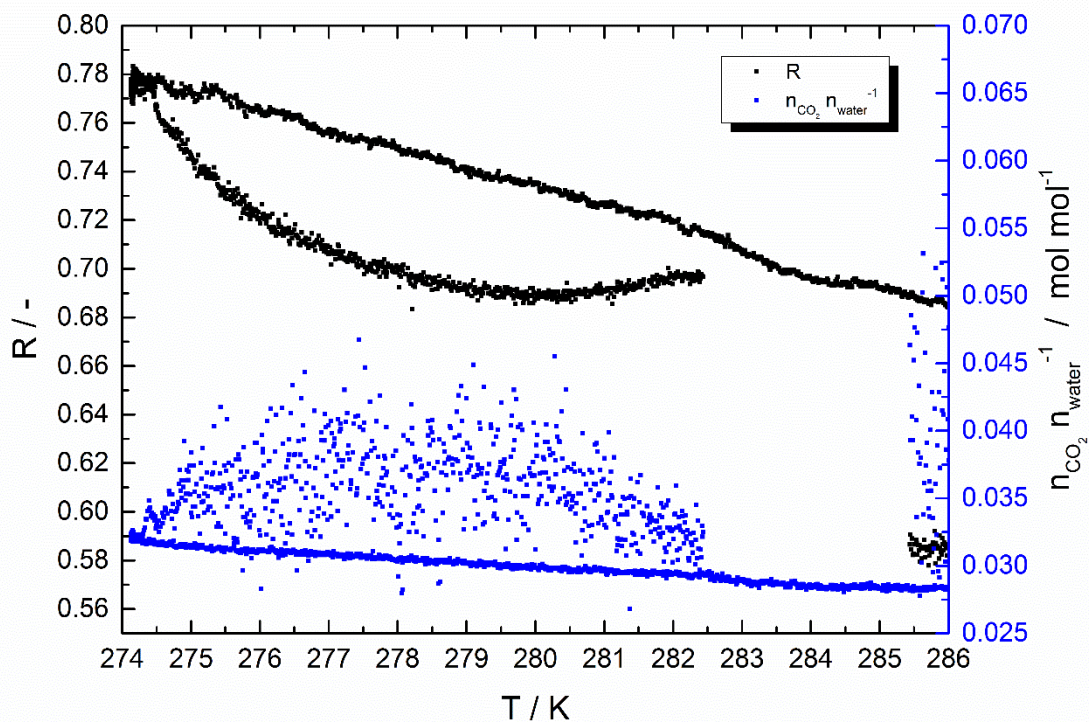

Figure C.9 Measurement 2 B (water, Luvicap PL (0.6 wt. %) and CO_2):CO_2 concentration in water and R-value versus temperature inside the cell

Figure C.10 Measurement 2 C (water, Luvicap PL (0.6 wt. %) and CO$_2$): Temperature inside the cell and the maximal intensity of the spectrum versus the time

Figure C.11 Measurement 2 C (water, Luvicap PL (0.6 wt. %) and CO$_2$):CO$_2$ concentration in water and R-value versus temperature inside the cell
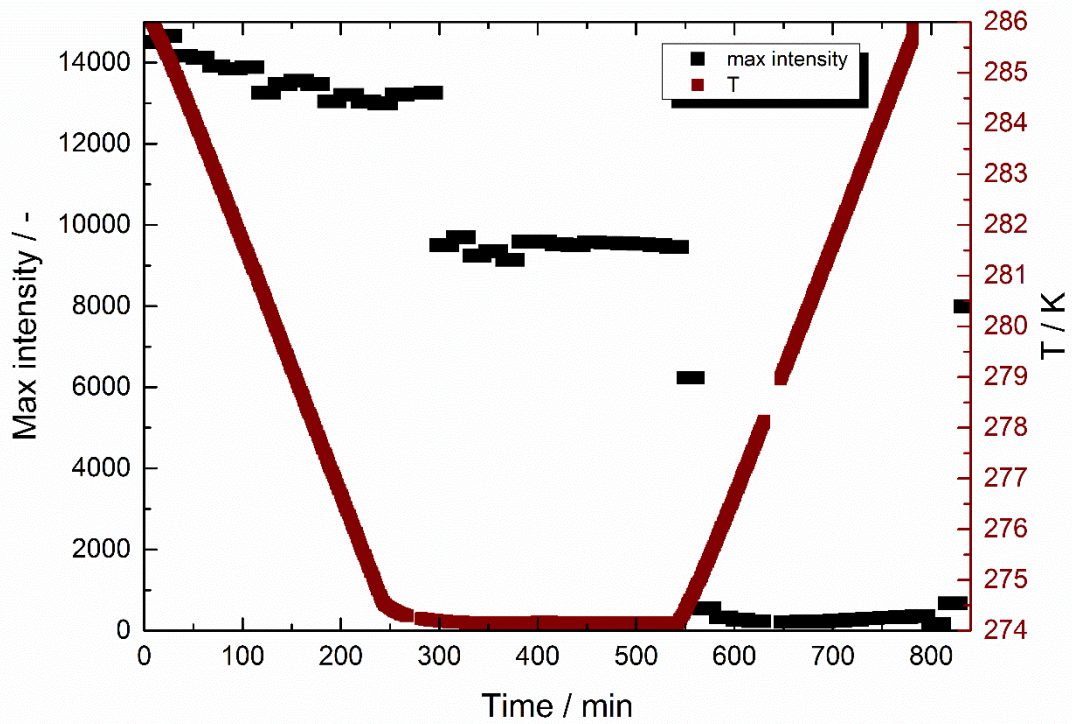
Figure C.12 Measurement 3 A (water, Luvicap 55W and CO_2): Temperature inside the cell and the maximal intensity of the spectrum versus the time
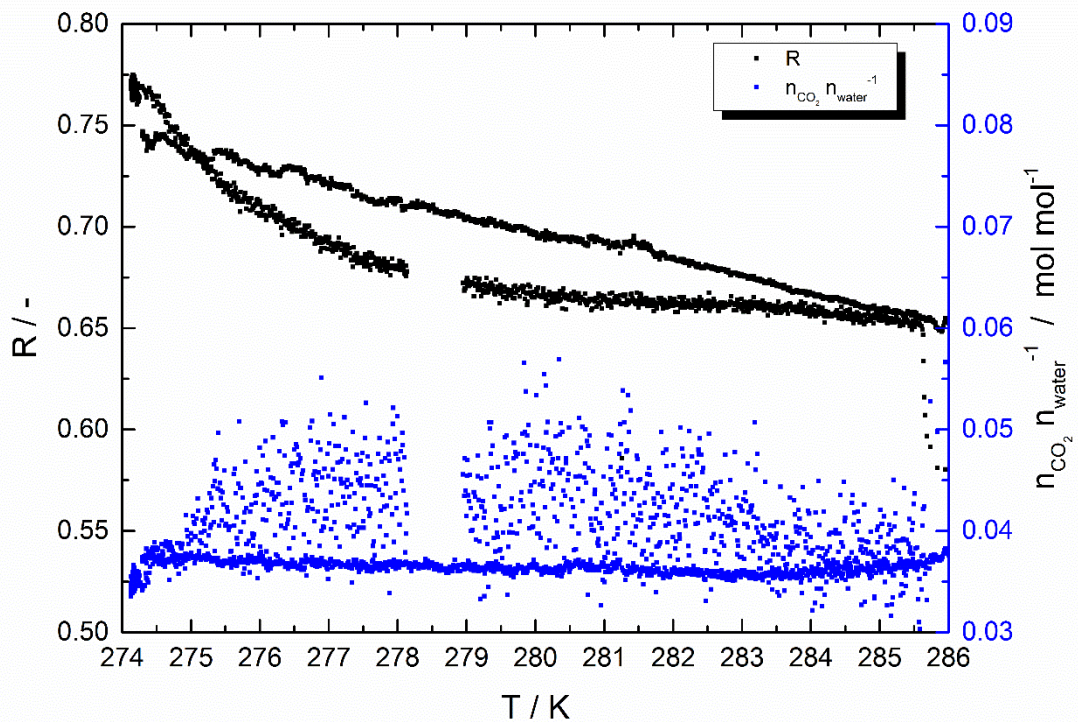

Figure C.13 Measurement 3 A (water, Luvicap 55W and CO_2):CO_2 concentration in water and R-value versus temperature inside the cell

Figure C.14 Measurement 3 B (water, Luvicap 55W and CO₂): Temperature inside the cell and the maximal intensity of the spectrum versus the time

Figure C.15 Measurement 3 B (water, Luvicap 55W and CO₂):CO₂ concentration in water and R-value versus temperature inside the cell
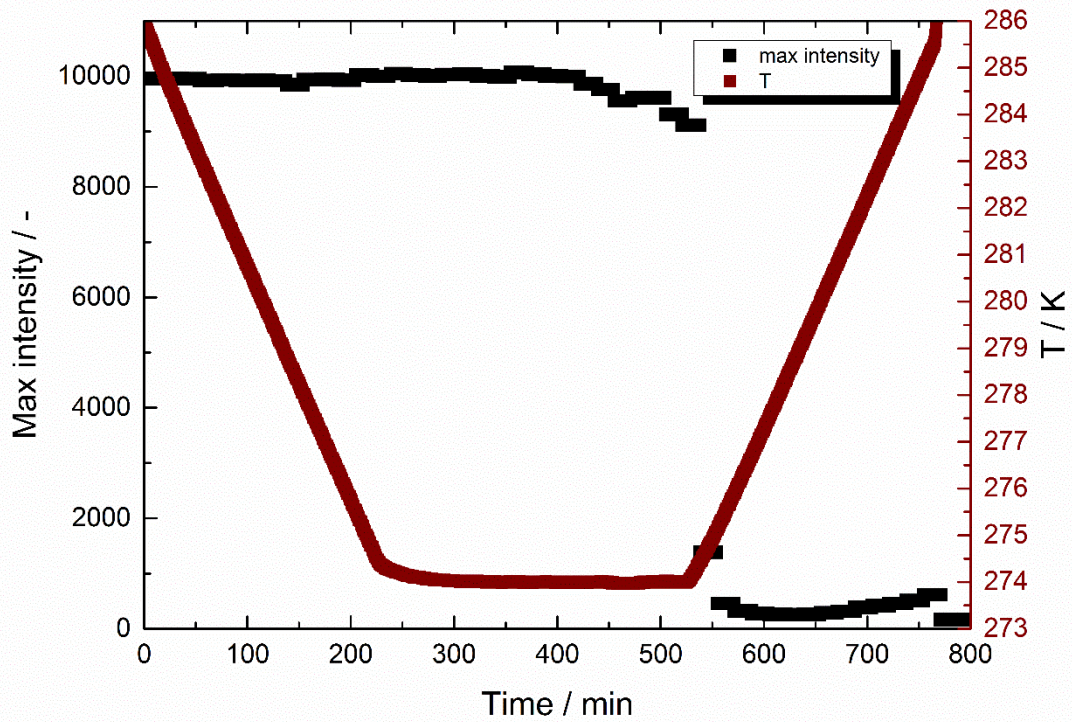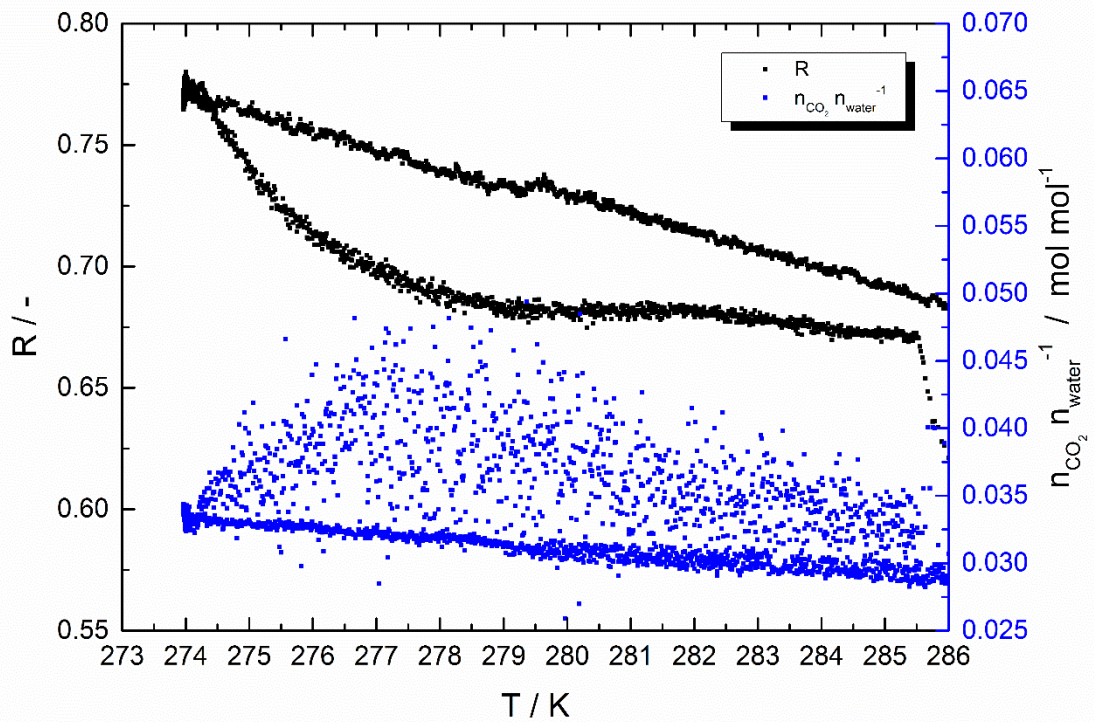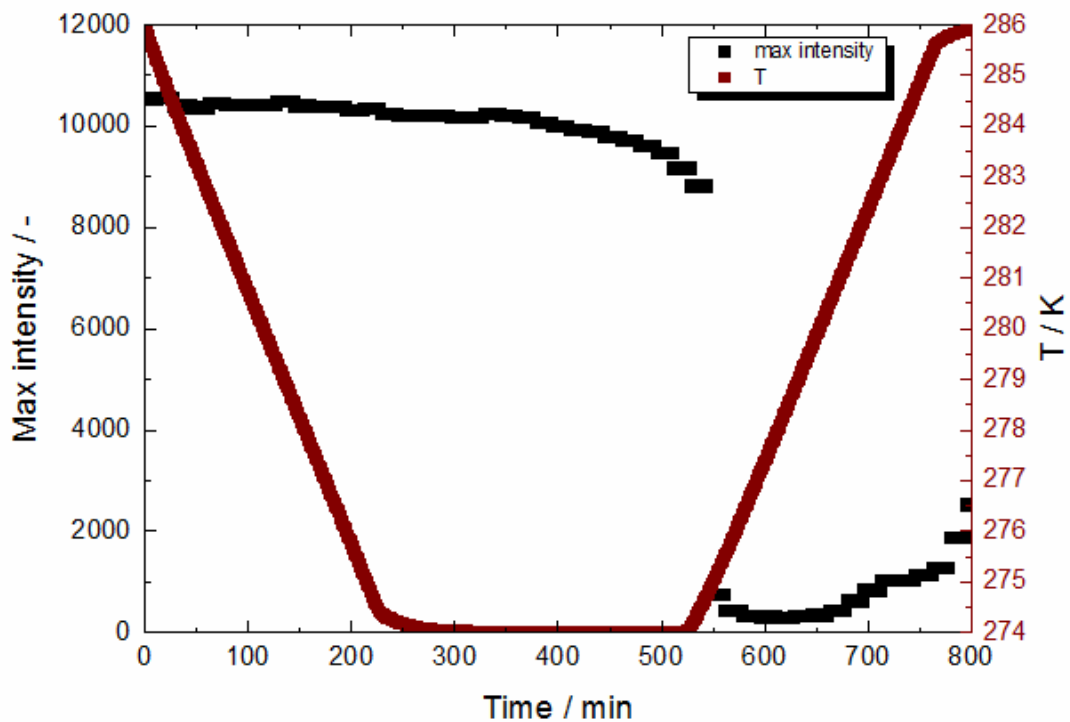
Figure C.16 Measurement 3 C (water, Luvicap 55W and CO_2): Temperature inside the cell and the maximal intensity of the spectrum versus the time
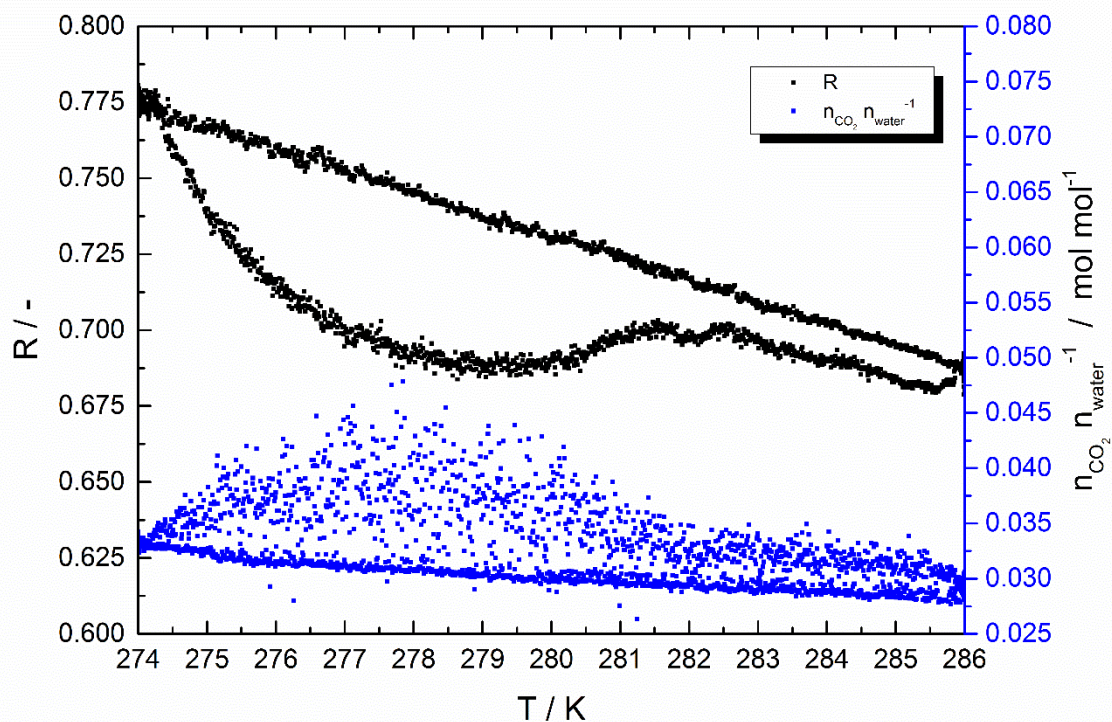

Figure C.17 Measurement 3 C (water, Luvicap 55W and CO_2):CO_2 concentration in water and R-value versus temperature inside the cell

Figure C.18 Measurement 4 A (water, Luvicap PL (1 wt. %) and CO_2): Temperature

inside the cell and the maximal intensity of the spectrum versus the time

Figure C.19 Measurement 4 A (water, Luvicap PL (1 wt. %) and CO_2):CO_2

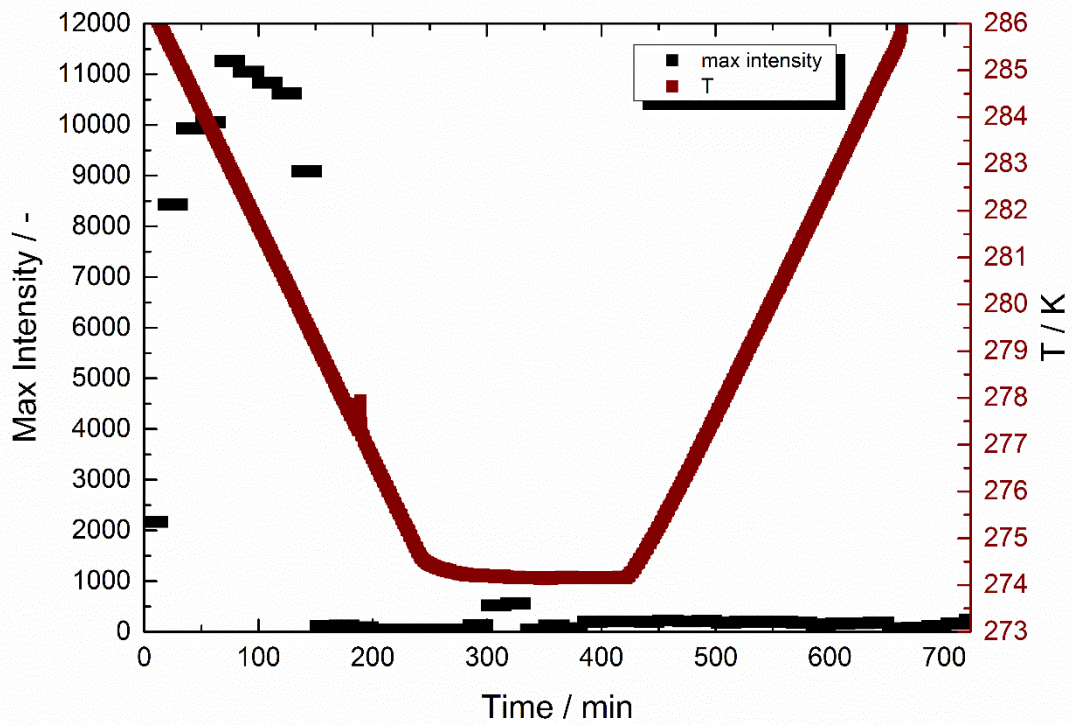*concentration in water and R-value versus temperature inside the cell*

Figure C.20 Measurement 4 B (water, Luvicap PL (1 wt. %) and CO₂): Temperature

inside the cell and the maximal intensity of the spectrum versus the time

Figure C.21 Measurement 4 B (water, Luvicap PL (1 wt. %) and CO₂):CO₂

concentration in water and R-value versus temperature inside the cell

Figure C.22 Measurement 4 C (water, Luvicap PL (1 wt. %) and CO₂): Temperature inside the cell and the maximal intensity of the spectrum versus the time
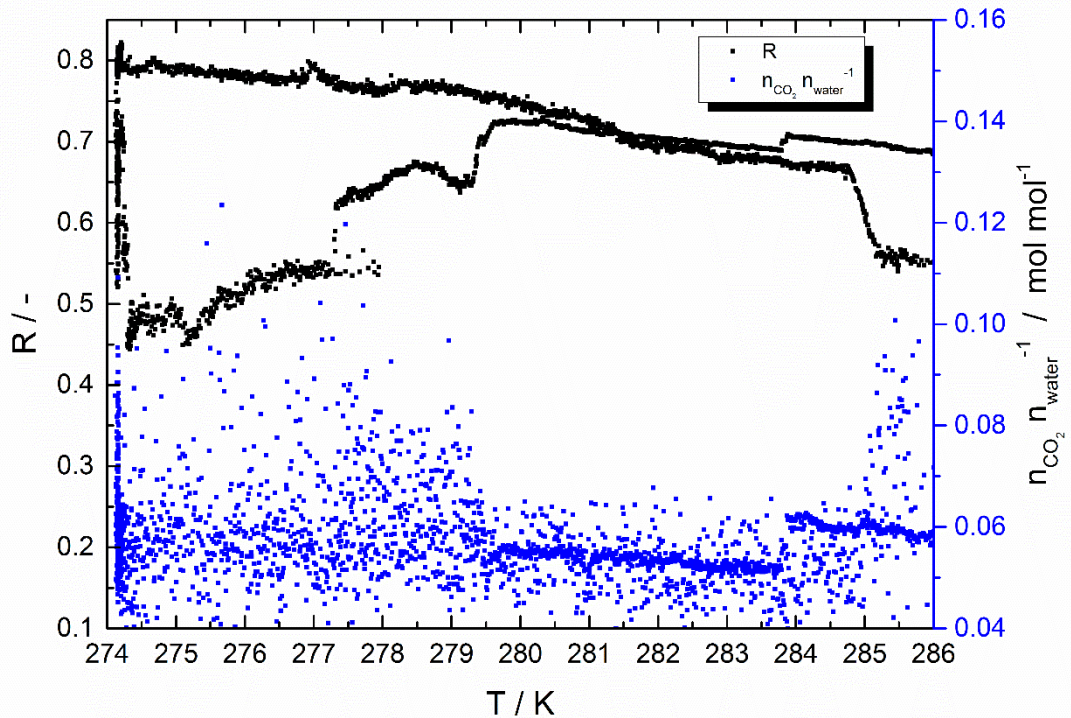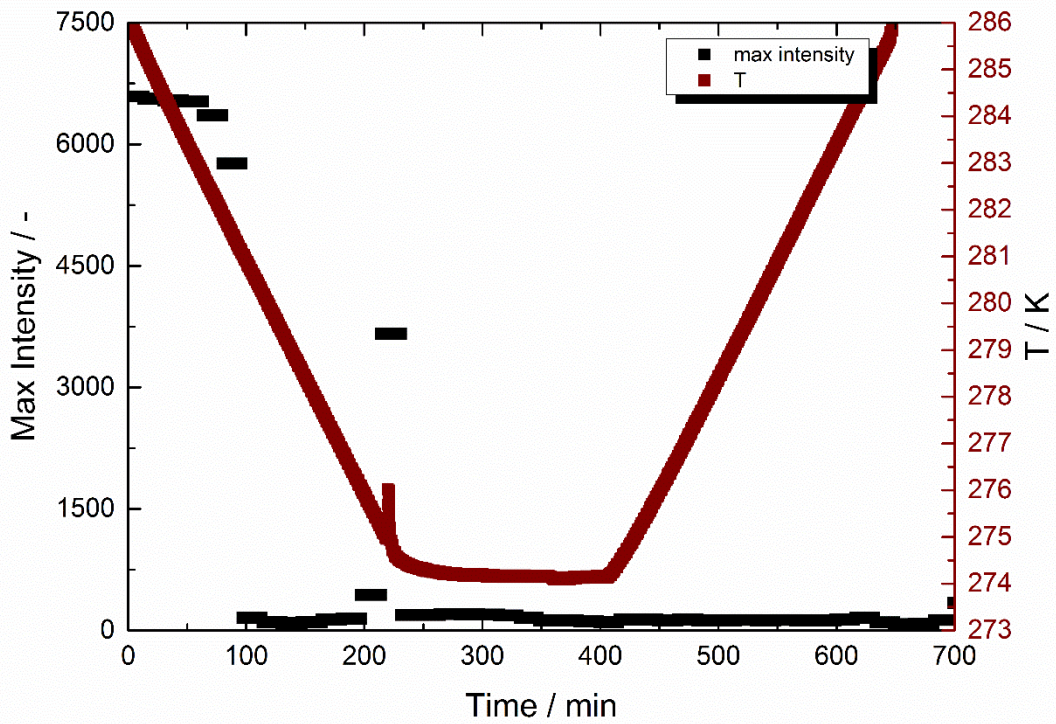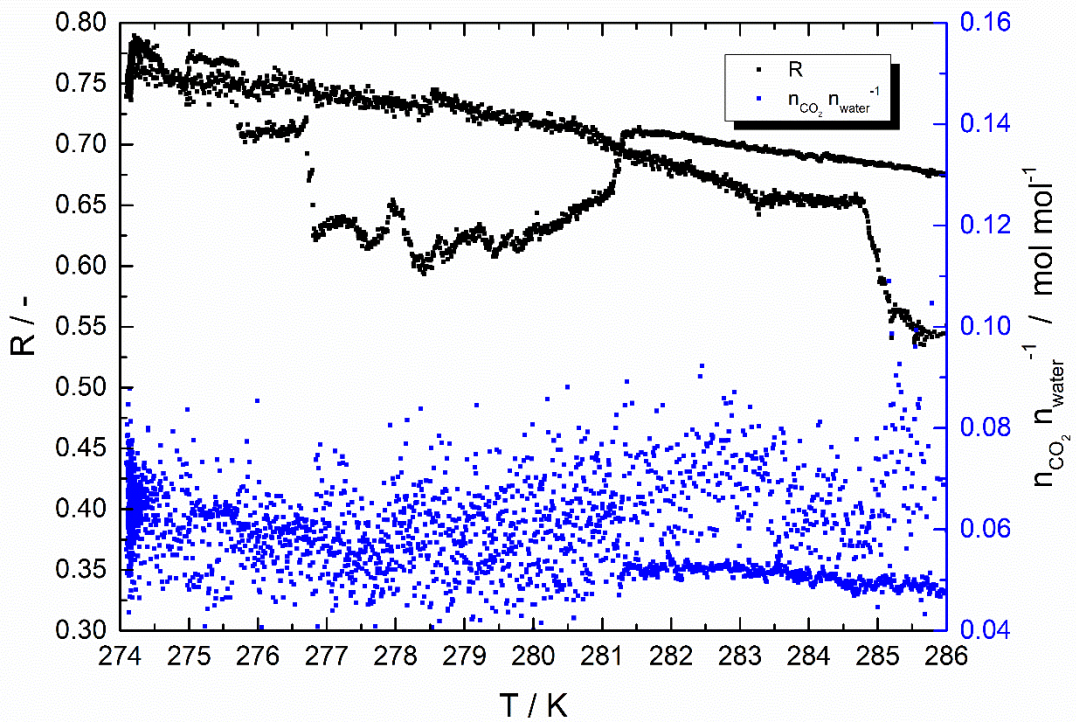

Figure C.23 Measurement 4 C (water, Luvicap PL (1 wt. %) and CO₂):CO₂ concentration in water and R-value versus temperature inside the cell

Figure C.24 Measurement 5 A (water, HI-M-PACT 85232 HCW and CO_2):
Temperature inside the cell and the maximal intensity of the spectrum versus the
time

Figure C.25 Measurement 5 A (water, HI-M-PACT 85232 HCW and CO_2):CO_2
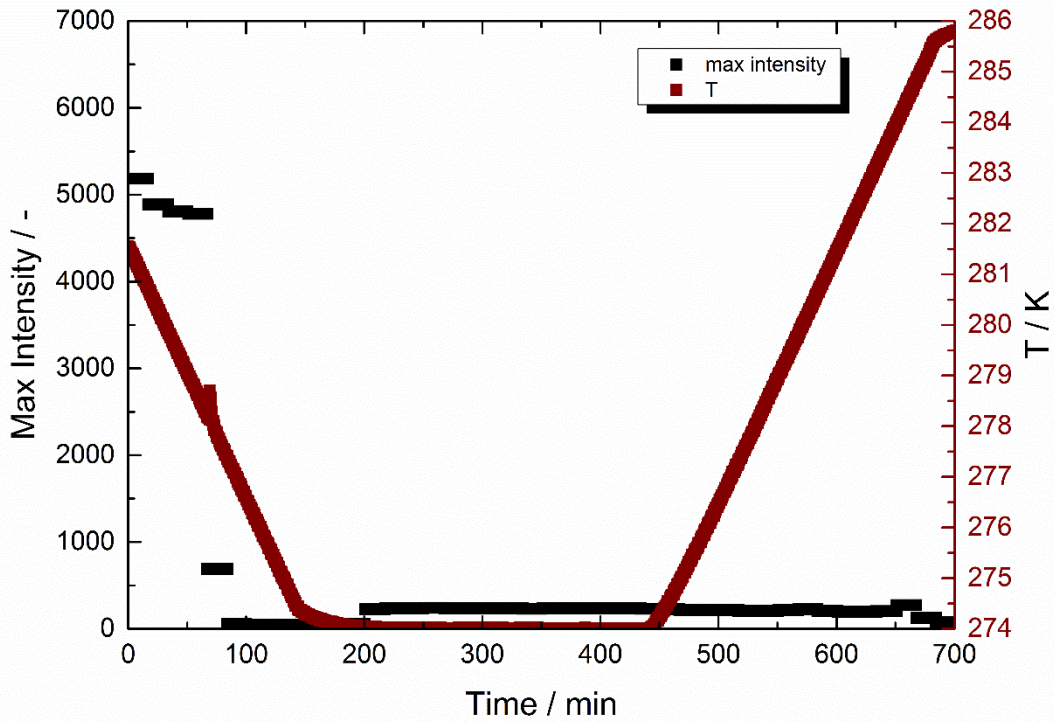*concentration in water and R-value versus temperature inside the cell*

Figure C.26 Measurement 5 B (water, HI-M-PACT 85232 HCW and CO_2): Temperature inside the cell and the maximal intensity of the spectrum versus the time

Figure C.27 Measurement 5 B (water, HI-M-PACT 85232 HCW and CO_2):CO_2 concentration in water and R-value versus temperature inside the cell

*Figure C.28 Measurement 5 C (water, HI-M-PACT 85232 HCW and CO_2):
Temperature inside the cell and the maximal intensity of the spectrum versus the
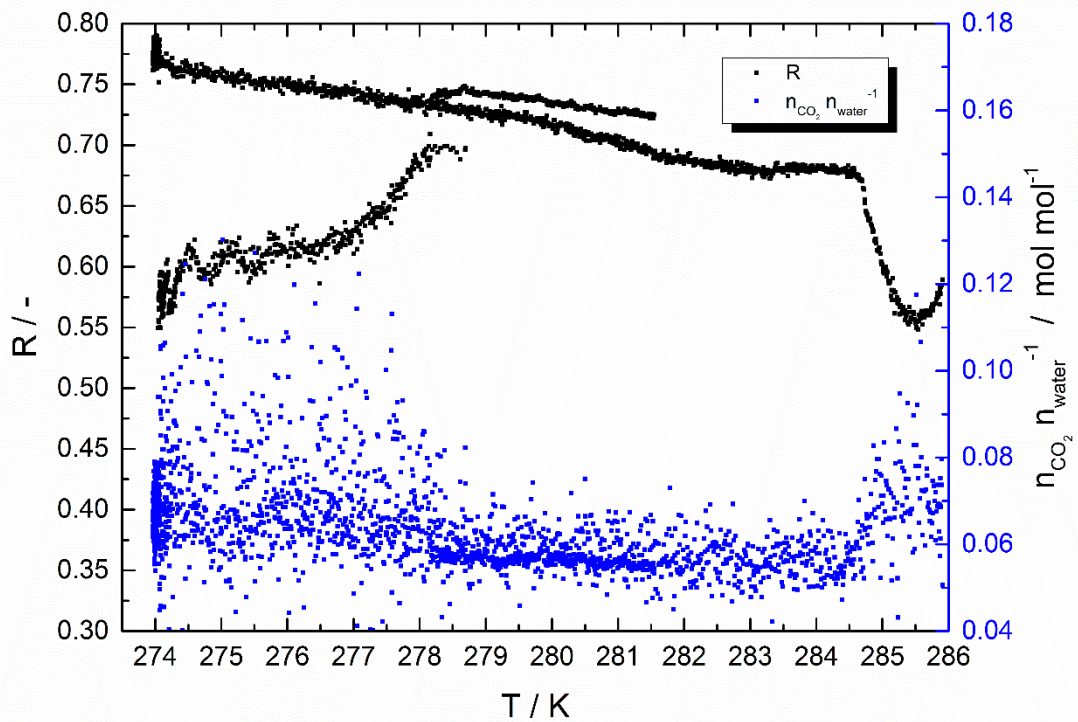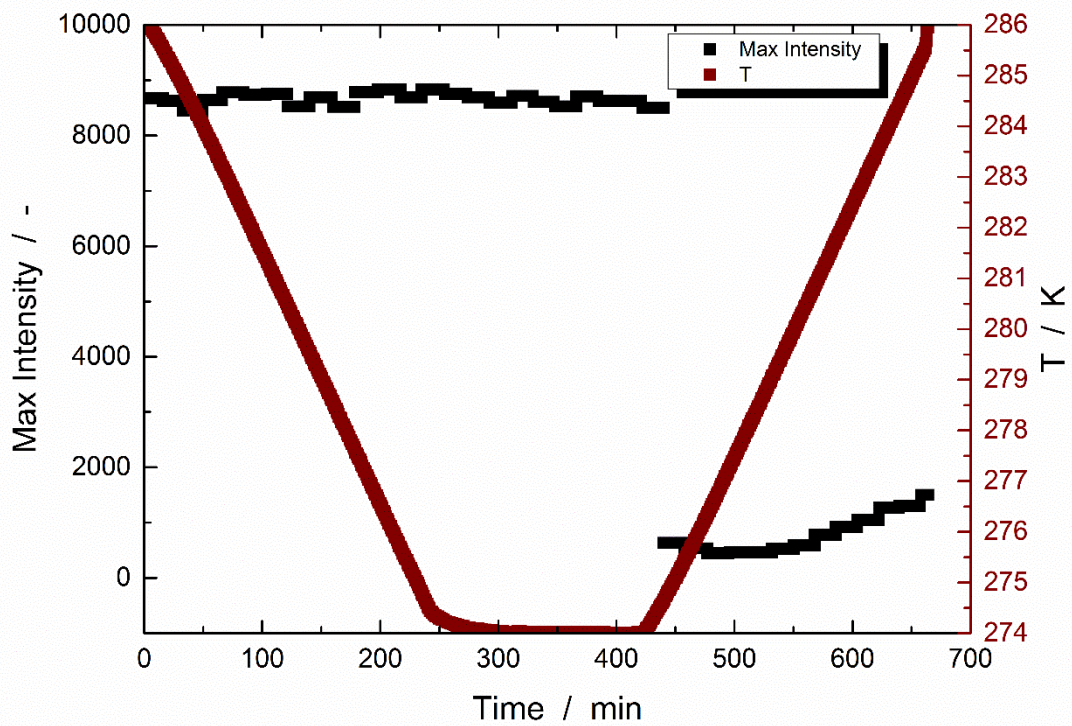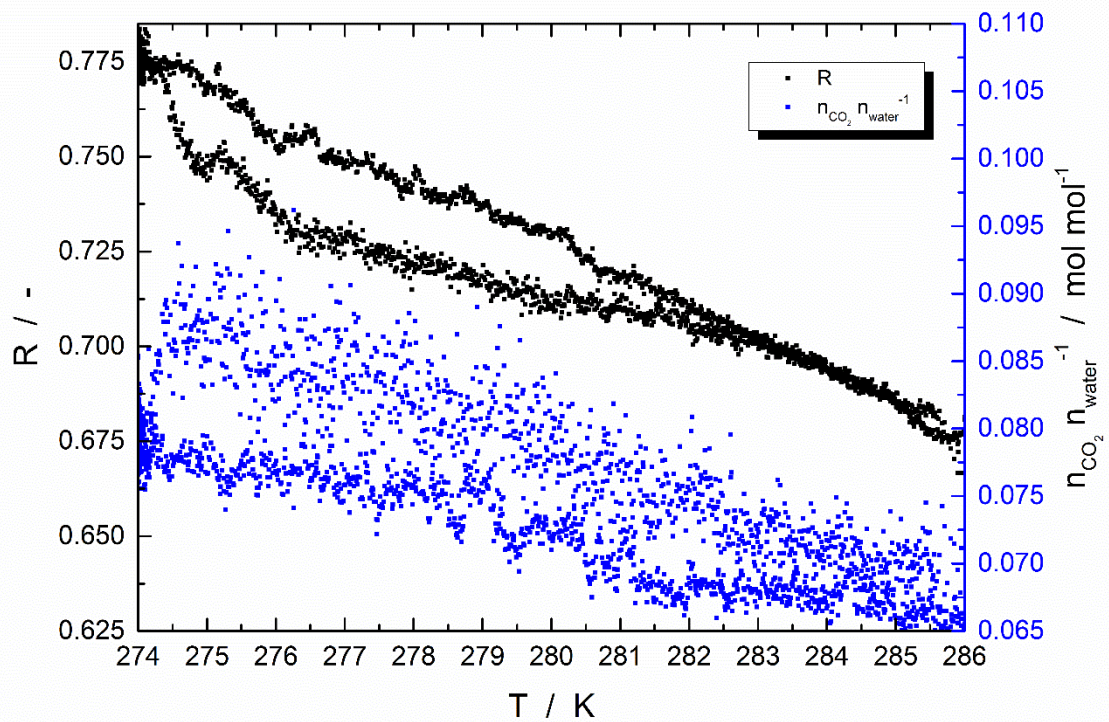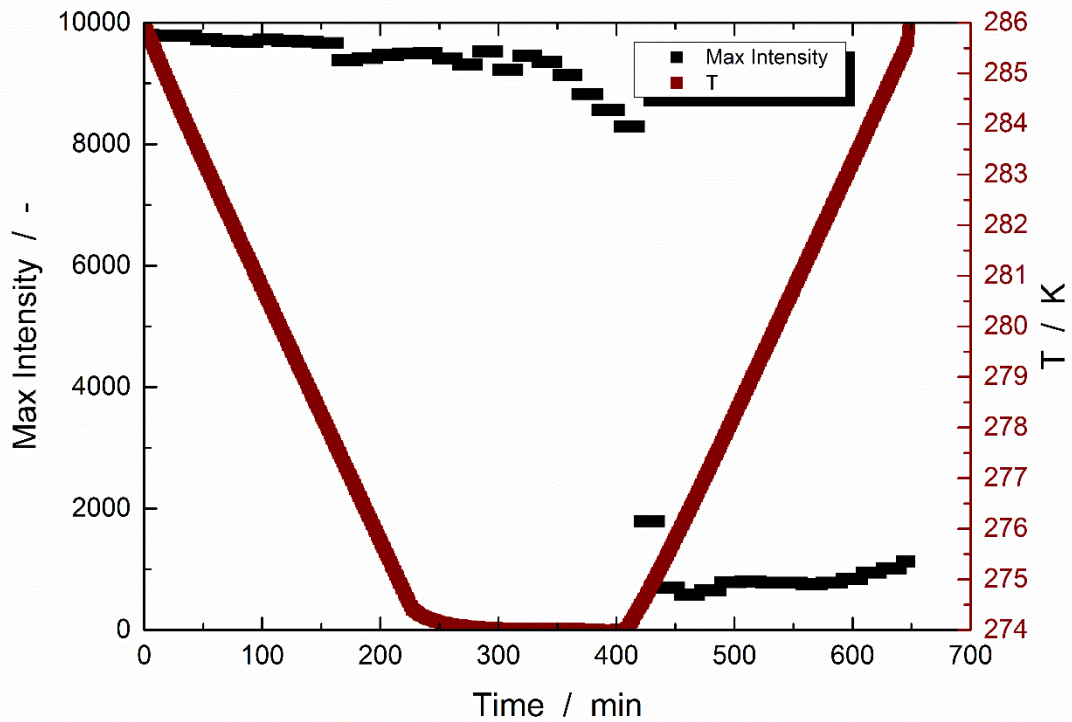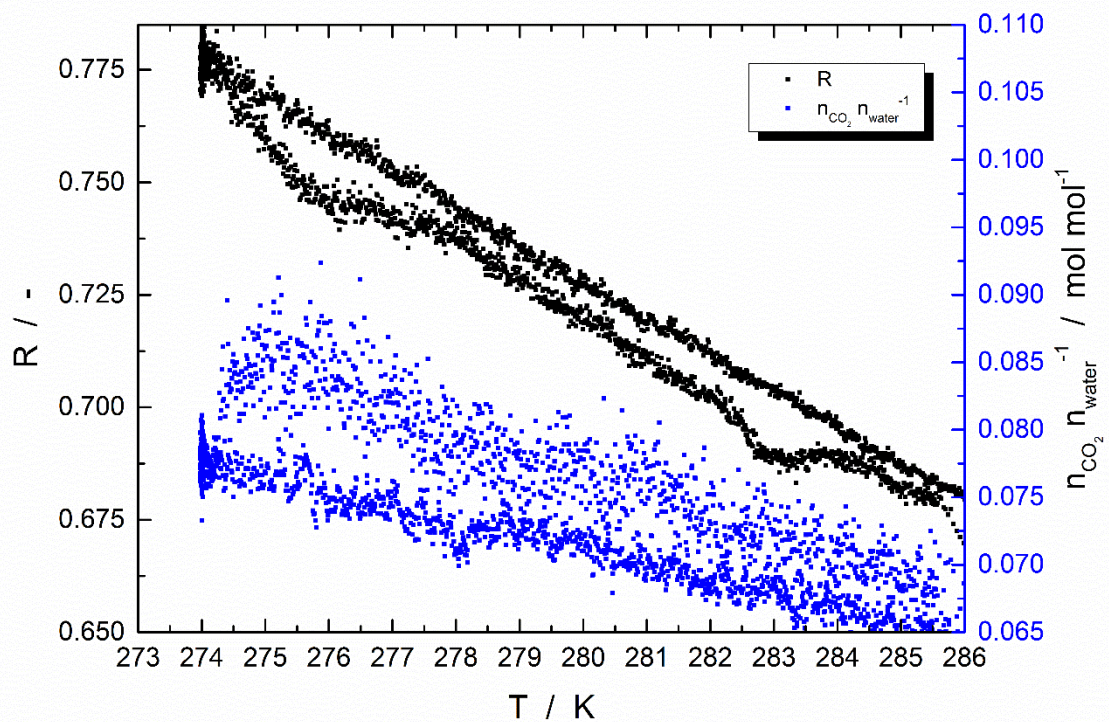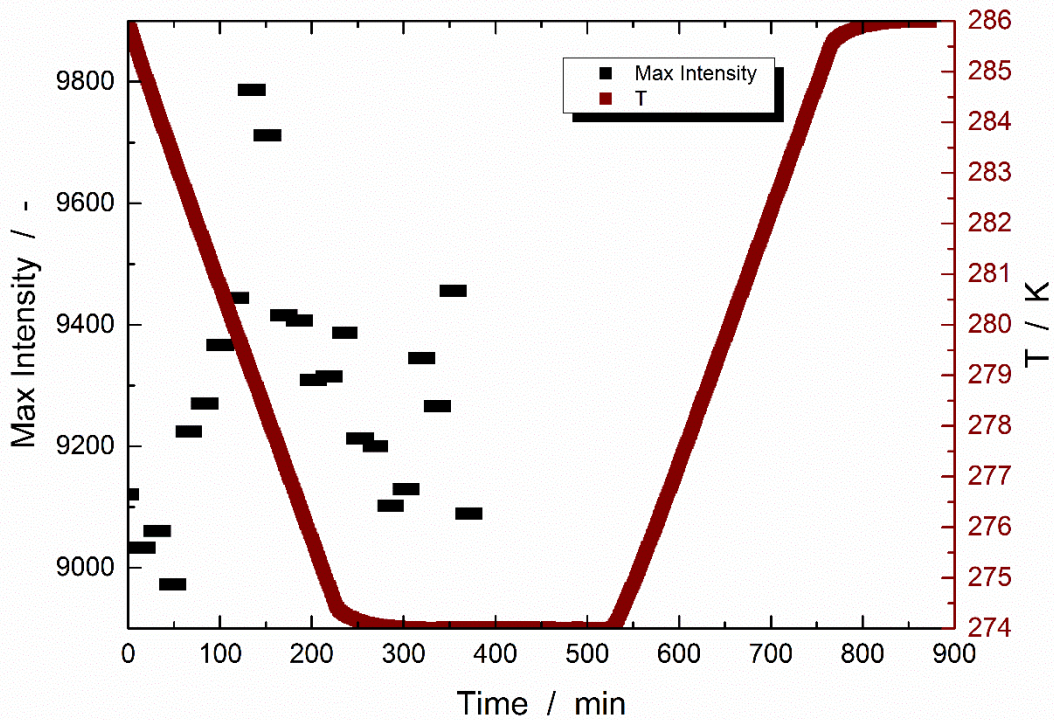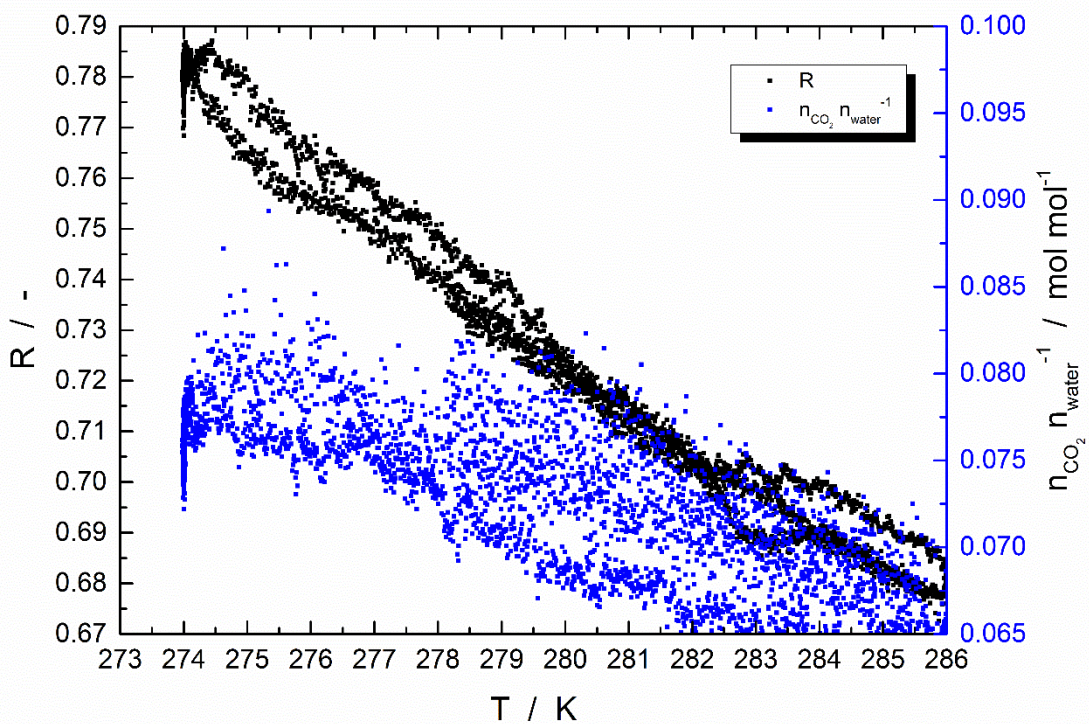time*

*Figure C.29 Measurement 5 C (water, HI-M-PACT 85232 HCW and CO_2):CO_2
concentration in water and R-value versus temperature inside the cell*

References

1. **Hammerschmidt E.G.**_Formation of gas hydrates in natural gas transmissions lines._ Texas : Ind. Eng. Chem. 26, 1934. (8) 851.

2. **Chatti I., Delahaye A., Fournaison L. and Petitet J.**_Benefits and drawbacks of clathrate hydrates: a review of their areas of interest._ s.l. : Energ. Convers. Manag, 2005. 46(9-10): 1333-1343.

3. **Giavarini C., Hester K.**_Gas Hydrates: Immense energy potential and environmental challenges._ London : Springer London, 2011.

4. **Sloan, E.D.**_Fundamental principles and applications of natural gas hydrates._ s.l. : Nature, 2003. 426(6964): p 353-363.

5. **Sloan E.D., Koh C.A.**_Clathrate hydrate of natural gases._ Boca Raton : CRC Press. 3rd ed., 2008. 721 .

6. **EnglezosP.**_Clathrates hydrates._ s.l. : Ind. Eng. Chem. Res., 1993. 32, 1251-1253.

7. **Scott-Hagen, C.E.T.** Hydrate inhibitors: alternatives to straight methanol injections. _Nothern Area Western Conf (NACE) International._ Calgary, Alberta, Canada, 2010, Publication Division, 1440 South Creek Drive, Houston, Texas 77084-4906.

8. **Storr M.T., et al.** Kinetic inhibitor of hydrate crystallization. _Journal of the American Chemical Society._ 2004, 126(5): p: 1569-1576.

9. **SloanE.D.**_A changing hydrate paradigm- from apprehension to avoidance to risk management._ s.l. : Fluid Phase Equilib, 2005. 228-229: 67.

10. **Davies S.R., Selim M.S., Sloan E.D., Bollavaram P. and Peters D.J.** Hydrate plug dissociation. _AIChE J._ 2006, 52:4016.

11. **Kamal M.S., Hussein I.A. , Sultan A.S.** Application of various water soluble polymers in gas hydrate inhibition. _Elsevier. Renewable and sustainable energy reviews._ 2016, 60 (2016) 206-225.

12. **Ramos J. C., Villanueva A.E., Ortiz C.M.** Espectroscopia Raman y sus aplicaciones. _Opt. Pura. Apl._ Tonantzintla, Puebla, México, 2013, 46 (1) 83-95 .

13. **Caspers P.J., Lucassen G.W., Wolthuis H., Bruining A., Puppels G.J.** In vitro and in vivo Raman spectroscopy of human skin. *Biospectroscopy.* 1998, 4, p. 31-39.

14. **Villanueva-Luna A.E., Castro-Ramos J., Vazquez-Montiel S., Flores Gil A., Delgado-Atencio J.A.** Comparison of different kinds of skin using Raman spectroscopy. *Proc. SPIE.* 2010, 7572, 75720M.

15. **Haka A.S., Shafer-Peltier K.E., Fitzmaurice M., Crowe J., Dasari, R.R., Feld M.S.** Identifying microcalcifications in benign and malignant breast lesions by probing differences in thier chemical composition using Raman spectroscopy. *Cancer Res.* 2002, 62, p. 5375-5380.

16. **Bartick E.G., Buzzini P.***Raman spectroscopy in forensic science.* Chichister : Encyclopedia of analytical chemistry, 2009. P: 5900-5915.

17. **J.L., Koening.***Infrared and raman spectroscopy of polymers.* Shrewsbury : s.n., 2001. Vol. Shrewsbury.

18. **C.S.S.R., Kumar.***Raman spectroscopy for nanomaterials characterization.* Berlin : Springer, 2012.

19. **Chung H., Ku M.S.** Comparison of near-infrare, infrared, and Raman spectroscopy for the analysis of heavy petroleum products. *Appl. Spectrosc.* 2000, 54, p. 239-245.

20. **Holzammer C., Finckenstein A., Will S., Braeuer A.S.** How sodium chloride salt inhibits the formation of CO2 gas hydrates. *The journal of physical chemistry B.* 2016, Vols. 120, 2452-2459.

21. **Braeuer A, Hankel R.F., Mehnert M.K., Schuster J.J. and Will S.** A Raman technique applicable for the analysis of the working principle of promoters and inhibitors of gas hydrate formation. *Journal of Raman Spectroscopy.* 2015, JRS 4744.

22. **Xu Y., Yang M., Yang X.** Chitosan as green kinetic inhibitors for gas hydrate formation. *Journal of Natural Gas Chemistry .* 2010, 19(4):431-435.

23. **Kashchiev D., Firooyabadi A.** Induction time in crystallization of gas hydrates. *Journal of Crystal Growth .* 2003, 250 (2003) 499-515.

24. **Delgado J.G.** *Hidratos de Gas. Cuaderno FIRP S363-A.* Universidad de los Andes. Mérida-Venezuela : FIRP, 2013.

25. **University, Heriot-Watt.** Heriot Watt Institute of Petroleum Engineering. *Where are gas hydrates found?* [Online] thehydrateforum.org. [Cited: July 27, 2016.] http://www.pet.hw.ac.uk/research/hydrate/hydrates_where.cfm.

26. **Sloan E.D., Sum A.K., Koh C.A., Crekk J.L., Ballard A.** *Natural gas hydrates in flow assurance.* Amsterdam : Elsevier XXII, 2011. 200 s.

27. **von Stackelberg, M.** Solid gas hydrates. *Naturwissenschaften.* 1949, 11-12, 1-22.

28. **Tang C., et. al.** *Kinetic studies of gas hydrate formation with low-dosage hydrate inhibitors.* s.l. : Science China Chemistry, 2010. 53(12) p:2622-2627.

29. **CoxJ.L.** *Natural gas hydrates: properties, occurrence and recovery.* Boston, Butterworth : VIII, 125s, 1983. 0250406314.

30. **MakogonJ.F.** *Hydrates of hydrocarbons.* Tulsa, Oklahoma : PennWell Books, 1997. XXX, 482s.

31. **Christiansen R.L., Sloan E.D.** Mechanisms and kinetics of hydrate formation. *Annals of the New York Academy of Science.* 1994, 715(1) p: 283-305.

32. **Fu S.B., Cenegy L.M., Neff C.S.** A summary of successful field applications of a kinetic hydrate inhibitor. *SPE International Symposium on Oilfield Chemistry.* 2001, Vols. Society of Petroleum Engineers Inc.: Houston, Texas.

33. **Mokhatab S., Poe W.A. and Speight J.G.** *Handbook of natural gas transmission and processing.* UK : Elsevier, 2006. 0-7506-7776-7.

34. **PetroWiki.** Petrowiki. *Predicting Hydrate Formation.* [Online] [Cited: April 29th, 2016.] http://petrowiki.org/Predicting_hydrate_formation.

35. **Hammerschmidt, E.G.** *Gas hydrate formations: A further study on their prevention and elimination from natural gas pipe lines.* s.l. : Gas, 1939. 15 (5) 30-35.

36. **Igboanusi U.P., Opara A.C.** The advancement from thermodynamic inhibitors to kinetic inhibitors and anti-agglomerants in natural gas flow assurance. *International Journal of Chemical and Environmental Engineering.* 2 (2), 2011, p: 131-134.

37. **Kelland, M.A.***Production chemicals for the oil and gas industry 2nd Ed.* s.l. : CRC Press, 2014. 9781439873793.

38. **Guan, H.** The inhibition of gas hydrates and synergy of the inhibiting molecules. *in International Oil and Gas Conference and Exhibition in China.* Beijing, China : Society of Petroleum Engineers, 2010.

39. **Nakarit, C.***Gas Hydrate Formation and Control by the Use of Chemicals.* Department of Mathematics and Natural Science : University of Stavanger. Faculty of Science and Technology, 2012.

40. **Kelland M.A., Del Villano L.** Tetrahydrofuran hydrate crystal growth inhibition by hyperbranched poly(ester amide) kinetic hydrate inhibitors- Evidence that polymer adsorption onto hydrate crystals is not the primary mechanism for gas hydrate inhibition by this polymer class. *Chem Eng Sci.* 2009, 64: 3197.

41. **Zeng H., Lu H., Huva E., Walker V.K.,Ripmeester J.A.** Differences in nucleator adsorption may explain distinct inhibition activities of two gas hydrate kinetic inhibitors. *Chem Eng Sci.* 2008, 63: 4026-9.

42. **Makogon T.Y., Sloan E.D.** Mechanism of kinetic hydrate inhibitors. *Proceedings of the 4th international conference on gas hydrates. Yokohama, Japan.* 2002, Vols. p: 498-503.

43. **Zeng H, Walker V.K., Ripmeester J.A.,.** Approaches to the design of better low-dosage gas hydrate inhibitors. *Angew. Chem.* 2007, 119: 5498-500.

44. **Englezos, P.** Nucleation and growth of gas hydrate crystals in relation to "kinetic inhibition". *Oil Gas Science Technology.* 1996, 51: 789-795.

45. **Carroll, J.J.***Natural Gas Hydrates: A Guide for Engineers.* Amsterdam : Elsevier XVII, 2009. 276s.

46. **Hawtin R.W., Rodger P.M.** Polydispersity in oligomeric low dosage gas hydrate inhibitors. *J. Mater Chem.* 2006, 16: 1934-1942.

47. **GamboaJ.A.***Espectroscopia NIR y RAMAN para el control de calidad en industria farmacéutica.* Universitat Autónoma de Barcelona. Facultad de Ciencias. Departamento de Química : s.n., 2014.

48. **Morales, G. L.***Caracterización óptica del ámbar de Chiapas. Diseño y construcción de un prototipo experimental para la autentificación del ámbar.* León, Guanajato : Centro de Investigaciones en Óptica A.C., 2012. 3.3 p. 37-40.

49. **Li Z., Deen M.J., Kumar S. and Selvaganapathy P.R.** Raman spectroscopy for in-line water quality monitoring — instrumentation and potential. School of Biomedical Engineering, Electrical and Computer Engineering and Mechanical Engineering, McMaster University, Hamilton, Canada; Electronic and Computer Engineering, Hong Kong, China, Septiembre 2014, Sensors 2014, 14, 17275-17303; doi:10.3390/s140917275.

50. **PérezR.***Procesado y optimización de espectros Raman mediante técnicas de lógica difusa: Aplicación a la identificación de materiales pictóricos.* Universitat Politécnica de Catalunya, BarcelonaTech : Departament de Teoria del Senyal i Comunicacions, 2005. 8468909696.

51. **Walrafen G.E., Hokmabadi M.S., Yang W.H.** Raman isosbestic points from liquid water. *The journal of chemical physics.* 1986, Vols. 85, 6964.

52. **Kelland M.A., Moi N., Howarth M.** Breakthrough in synergists for kinetic hydrate inhibitor polymers, hexaalkylguanidinium salts: Tetrahydrofuran hydrate crystal growth inhibition and synergism with polyvinylcaprolactam. *American Chemical Society.* 2013, Vol. 27(2), p:711-716.

53. **Posteraro D., Ivall J., Maric M., Servio P.** New insights into the effect of PVP concentration on methane hydrate growth. 2. liquid phase methane mole fraction. *Chemical Engineering Science.* Elsevier, 2015, 126, p: 91-98.

54. **Chua P. C., Kelland M., O´Reilly R., Ieong N. S.** The missing poly(n-vinyl lactam) kinetic hydrate inhibitor- Part 1. Crystarl growth inhibition of tetrahydrofuran hydrate with poly(n-vinyl piperidone) and other poly(n-vinyl lactam) homopolymers. *Proceedings of the 7th International Conference on Gas Hydrates .* Edingburgh, Scotland, United Kingdom, 2011, (ICGH 2011).

55. **Lee J.D., Wu H., Englezos P.** Cationic starches as gas hydrate kinetic inhibitors. *Chemical Engineering Science.* Elsevier, 2007, 62; p: 6548-6555.